Cellular/Molecular

The Gain-of-Function Integrin β3 Pro33 Variant Alters the Serotonin System in the Mouse Brain

Michael R. Dohn,[1] Christopher G. Kooker,[1] Lisa Bastarache,[2] Tammy Jessen,[1,5] Capria Rinaldi,[1] Seth Varney,[1] Matthew D. Mazalouskas,[1] Hope Pan,[1] Kendra H. Oliver,[1] Digna R. Velez Edwards,[3,5] James S. Sutcliffe,[4,5] Joshua C. Denny,[2,5] and Ana M.D. Carneiro[1]

Departments of [1]Pharmacology, [2]Biomedical Informatics and Medicine, [3]Obstetrics and Gynecology, and [4]Psychiatry and Molecular Physiology & Biophysics, and [5]Vanderbilt Genetics Institute, Department of Obstetrics and Gynecology, Vanderbilt University, Nashville, Tennessee 37232

Engagement of integrins by the extracellular matrix initiates signaling cascades that drive a variety of cellular functions, including neuronal migration and axonal pathfinding in the brain. Multiple lines of evidence link the *ITGB3* gene encoding the integrin β3 subunit with the serotonin (5-HT) system, likely via its modulation of the 5-HT transporter (SERT). The *ITGB3* coding polymorphism Leu33Pro (rs5918, Pl^{A2}) produces hyperactive αvβ3 receptors that influence whole-blood 5-HT levels and may influence the risk for autism spectrum disorder (ASD). Using a phenome-wide scan of psychiatric diagnoses, we found significant, male-specific associations between the Pro33 allele and attention-deficit hyperactivity disorder and ASDs. Here, we used knock-in (KI) mice expressing an *Itgb3* variant that phenocopies the human Pro33 variant to elucidate the consequences of constitutively enhanced αvβ3 signaling to the 5-HT system in the brain. KI mice displayed deficits in multiple behaviors, including anxiety, repetitive, and social behaviors. Anatomical studies revealed a significant decrease in 5-HT synapses in the midbrain, accompanied by decreases in SERT activity and reduced localization of SERTs to integrin adhesion complexes in synapses of KI mice. Inhibition of focal adhesion kinase (FAK) rescued SERT function in synapses of KI mice, demonstrating that constitutive active FAK signaling downstream of the Pro32Pro33 integrin αvβ3 suppresses SERT activity. Our studies identify a complex regulation of 5-HT homeostasis and behaviors by integrin αvβ3, revealing an important role for integrins in modulating risk for neuropsychiatric disorders.

Key words: FAK; focal adhesion; integrin beta3; ITGB3; serotonin; SERT

Significance Statement

The integrin β3 Leu33Pro coding polymorphism has been associated with autism spectrum disorders (ASDs) within a subgroup of patients with elevated blood 5-HT levels, linking integrin β3, 5-HT, and ASD risk. We capitalized on these interactions to demonstrate that the Pro33 coding variation in the murine integrin β3 recapitulates the sex-dependent neurochemical and behavioral attributes of ASD. Using state-of-the-art techniques, we show that presynaptic 5-HT function is altered in these mice, and that the localization of 5-HT transporters to specific compartments within the synapse, disrupted by the integrin β3 Pro33 mutation, is critical for appropriate reuptake of 5-HT. Our studies provide fundamental insight into the genetic network regulating 5-HT neurotransmission in the CNS that is also associated with ASD risk.

Introduction

Dysregulation of serotonin [5-hydroxytryptamine (5-HT)] homeostasis in the CNS plays a key role in depression and anxiety disorders (Ruhé et al., 2007) and has long been implicated in developmental abnormalities of autism spectrum disorder (ASD; Cook and Leventhal, 1996; Jaiswal et al., 2015). 5-HT is released from the presynaptic terminal to activate specific receptors and is

Received May 29, 2017; revised Aug. 21, 2017; accepted Aug. 22, 2017.

Author contributions: D.R.V.E., J.S.S., J.C.D., and A.M.D.C. designed research; M.R.D., C.G.K., L.B., T.J., C.R., S.V., M.D.M., H.P., K.H.O., J.C.D., and A.M.D.C. performed research; D.R.V.E., J.S.S., and A.M.D.C. contributed unpublished reagents/analytic tools; M.R.D., C.G.K., L.B., T.J., S.V., M.D.M., H.P., J.C.D., and A.M.D.C. analyzed data; M.R.D., M.D.M., J.S.S., and A.M.D.C. wrote the paper.

Pro32Pro33 KI mice were funded by an Autism Speaks Pilot Grant to J.S.S. This study was supported by National Institutes of Health (NIH) Grant MH-090256 (M.R.D., T.J., and A.M.D.C.), Vanderbilt Postdoctoral Training Grant in Functional Neurogenomics Grant T32-MH65215 (M.D.M.), American Heart Association Predoctoral Fellowship 14PRE19640007 (K.H.O.), and NIH Grant R01-LM-010685 (L.B. and J.C.D.). C.R. performed OMX image processing and data analysis and was supported by the Vanderbilt Summer Science Academy. The contributions of C.G.K., S.V., and H.P. were supported by the Vanderbilt University Interdisciplinary Program in Neuroscience for Undergraduates. BioVU is supported by institutional funding and by the Vanderbilt CTSA Grant ULTR000445 from NCATS/NIH. The Zeiss confocal and OMX microscopes are housed in the Vanderbilt Cell Imaging Shared Resource supported by NIH Grants CA-68485, DK-20593, DK-58404, DK-59637, and EY-08126. We thank John Allison for assistance with training our students in behavioral tests and general administration and organization of the Vanderbilt Murine Neurobehavioral Core. We also thank Dr. Randy Blakely for his input and assistance in the early stages of the project. In addition, we thank Nivedita Kukreti for requantifying the OMX images.

cleared from the synaptic cleft by the plasma membrane 5-HT transporter (SERT; Blakely et al., 1998). Uptake of 5-HT by SERT not only replenishes neuronal stores of 5-HT but also dictates the strength and duration of serotonergic transmission, thus underscoring the critical role that SERT plays in maintaining serotonergic homeostasis. SERT interacts with and is regulated by multiple proteins, including integrins (Carneiro et al., 2008; Oved et al., 2013; Whyte et al., 2014; Mazalouskas et al., 2015), A_3 adenosine receptors (Zhu et al., 2011), syntaxin (Quick, 2002; Ciccone et al., 2008), and α-synuclein (Wersinger et al., 2006). Clinically, the serotonergic system is regulated with selective 5-HT reuptake inhibitors (SSRIs) that directly block SERT function and permit sustained 5-HT signaling. SSRIs are widely used to treat psychiatric disorders, including depression, obsessive-compulsive disorder, and ASD (Schatzberg, 2000; Zohar et al., 2000a,b; Zohar and Westenberg, 2000; Jaiswal et al., 2015).

There are several lines of evidence that link the *ITGB3* gene, which encodes the integrin β3 subunit, with the 5-HT system (Weiss et al., 2004, 2006a,b; Coutinho et al., 2007). In platelets, integrin β3 heterodimerizes with integrin αIIb and physically interacts with SERT, dynamically modulating its uptake capacity and plasma membrane expression (Carneiro et al., 2008). In the brain, integrin β3 heterodimerizes with integrin α_V to form the vitronectin receptor (McGeachie et al., 2011), which colocalizes with SERT in midbrain presynaptic terminals (Mazalouskas et al., 2015). The *ITGB3* coding polymorphism rs5918 (Pl^{A2}, Leu33Pro) has been associated with elevated blood 5-HT levels and autism (Weiss et al., 2004, 2006a). This polymorphism results in a missense substitution of a leucine to proline at residue 33 of the mature β3 subunit; in the human protein, this creates adjacent proline residues at positions 32 and 33 (Pro32Pro33), which permits increased flexibility of the β3 extracellular domain and confers enhanced integrin receptor signaling (Vijayan et al., 2003b; Jallu et al., 2012). Increased platelet adhesion is observed in human patients with this polymorphism (Vijayan et al., 2003a), which is recapitulated in knock-in (KI) mice expressing the Pro32Pro33 variant of mouse integrin β3 (Oliver et al., 2014). These effects result from enhanced binding avidity of the receptor, which promotes the activation of intracellular signaling pathways (Vijayan et al., 2003b; Oliver et al., 2014). Interestingly, SERT activity is upregulated following coexpression of the human Pro33 variant in HEK293 cells (Carneiro et al., 2008), suggesting that enhanced integrin β3 signaling modifies 5-HT blood levels at least in part via regulation of SERT function.

While the role of the Pro33 variant has been studied in the periphery, the functional and biochemical consequences of this mutation in the brain remain unknown. In this study, we used the KI mouse model, in which the Pro32Pro33 variant of mouse integrin β3 is expressed from the endogenous integrin β3 locus (Oliver et al., 2014) to examine the effect of this mutation on the 5-HT system in the brain. Genetic studies in humans demonstrated that this polymorphism significantly contributes to alterations in phenotypes that are relevant to neuropsychiatric disorders, effects that are recapitulated in the KI mouse model. We extended our studies to the brain 5-HT system, revealing alterations in 5-HT synapses that culminate with altered intracellular signaling and reduced SERT function. Our studies reveal a complex regulation of 5-HT homeostasis by *ITGB3*, indicating an important role for integrins in modulating risk for neuropsychiatric conditions.

Materials and Methods

Phenome-wide association study. The phenotypes were constructed from electronic health record data aggregated from International Classification of Disease, ninth edition-Clinical Modification (ICD-9-CM) codes (Health Care Financing Administration, 1990) into phenome-wide association study (PheWAS) codes, corresponding to specific disease phenotypes, each with a control group defined as previously described (Denny et al., 2013). Case patients were defined as individuals who had at least two annotations of the same PheWAS code from two different visits. Individuals who only had one code or a code for a similar disease were excluded from control subjects. Logistic regression analyses were run using an additive model for rs5918, adjusted for age and stratified by gender and then tested for association across 25 prespecified PheWAS codes corresponding to neuropsychiatric conditions. Data are reported as raw numbers, and p values were not corrected for multiple testing using $\alpha = 0.002$.

Reagents. [^{3}H] 5-HT, [^{3}H] dopamine, and [^{3}H] citalopram radioligands were purchased from PerkinElmer Life Sciences, and paroxetine hydrochloride hemihydrate was purchased from Sigma-Aldrich. Antibodies used include guinea-pig anti-SERT (Frontier Institute; RRID:AB_2571777,), mouse anti-Na^+/K+ATPase α-1 (Millipore; RRID:AB_309699), rabbit anti-mouse integrin β3 (Cell Signaling Technology; RRID:AB_10695305), mouse anti-SNAP25 (Millipore; RRID:AB_11211926), rabbit anti-phosphorylated focal adhesion kinase (pFAK; Y397, Cell Signaling Technology; RRID:AB_10891442), mouse anti-talin (Sigma-Aldrich; RRID:AB_477572), and mouse anti-synaptophysin (Millipore; RRID:AB_95187). All secondary antibodies were purchased from Jackson ImmunoResearch. Src inhibitor SKI-606 was purchased from Sigma-Aldrich and FAK inhibitor PF-573228 was purchased from Bio-Techne.

Animals. Mouse studies were performed in accordance with humane guidelines established by the Vanderbilt Institutional Animal Care and Use Committee under approved protocols (M/12/167 and M/15/014). All animals used in this study were male mice (8–20 weeks of age) generated from crosses of heterozygous for the Pro32Pro33 knock-in *Itgb3* allele made on the C57BL/6 background (Oliver et al., 2014). Mice were group housed with their littermates, were maintained on a 12 h light/dark cycle, and were provided with food and water *ad libitum*.

Only homozygous animals were used in the analyses, even if heterozygous mice were run in behavioral experiments. Three cohorts of 11–16 mice underwent the first battery of behavioral assays for a total of 42 animals. All mice were initially housed with their littermates of the same sex in the Vanderbilt Murine Neurobehavioral Core, with controlled 12 h light/dark cycles, freely available food and water, and controlled temperature and humidity. The experimenter was initially blinded to the genotype of each animal, and each animal underwent the same battery of behavioral tests to establish phenotype. The order of behavioral tests was as follows: sociability test, social preference test, social reciprocity test, marble burying, and olfaction test. Mice remained at the Vanderbilt Murine Neurobehavioral Core but were individually housed during the olfaction test. Two other cohorts of animals totaling 57 mice were used for elevated zero maze, open field, tail suspension, and forced swim tests. The behavioral tests were administered in the same order for every animal, with animals being subjected to no more than one test per day.

Open field test. The open field test was used to examine locomotor activity and anxiety-related behavior. The apparatus, purchased from Med Associates, consisted of a square box (27.3 × 27.3 cm). The apparatus was placed in a sound-attenuating chamber purchased from Med Associates Horizontal and vertical arrays of 16 infrared beams tracked horizontal and vertical movements. The arena was brightly lit throughout the test. In the novelty testing, naive animals were placed in the center of the arena and allowed to explore the chamber for 10 min. The habituation testing was performed on the day after the novelty testing, where mice were reintroduced to the arena and allowed to explore for 10 min.

The authors declare no competing financial interests.

Correspondence should be addressed to Ana M. D. Carneiro, Department of Pharmacology, 2220 Pierce Avenue, Nashville, TN 37232. E-mail: ana.carneiro@vanderbilt.edu.

T. Jessen's present address: Department of Biology, Middle Tennessee State University, Murfreesboro, TN 37132.

DOI:10.1523/JNEUROSCI.1482-17.2017

 0270-6474/17/3711272-14$15.00/0

Open Field Activity software (Med Associates) was used to track and analyze the movements of the animals.

Elevated zero maze. Mice were placed on an elevated circular track apparatus ~65 cm in diameter. Two open zones and two closed zones, of equal length and all evenly spaced, were contained on the circular track. One mouse was placed in the middle of an open zone and allowed to explore the maze for 5 min. Video of the mouse was obtained and analyzed using ANY-maze software (Stoelting) for the amount of time spent in each zone, the number of entries into each zone, and the distances traveled. Entry of a zone was digitally quantified based on the criterion of ≥70% of the body of the animal being in a zone.

Forced swim test. Mice were placed in a clear cylinder with 23°C water ~20 cm deep and tested for 6 min. Mice were then placed in a clean heated cage for 15 min. Water was changed, and the apparatus was cleaned with chlorine dioxide between each test. All tests were filmed by video camera. Immobility was defined as the animal making minimal movements to keep its head above water, and a blind competent observer scored immobility. Latency to first immobile period, sum of immobility per minute, and total immobility were recorded. The total immobility time in the last 4 min of the test was the primary measure analyzed.

Tail suspension test. An automated tail suspension test device (Med Associates) was used to measure the duration of behavioral immobility. Mice were suspended by the tail with tape to a vertical aluminum bar connected to a strain gauge. Before attaching the tail to the bar, the tail was passed through a clear 3 cm plastic tube to prevent mice from climbing their own tails. The following settings were used in all experiments: threshold, 1:7; gain, 8; time constant, 0.25; and resolution, 200 ms. Immobility was recorded for 6 min.

Marble burying. A novel cage was prepared with a layer of Harlan T.7089 Diamond Soft bedding (Harlan Laboratories) covering the floor. This layer was 3 cm thick to allow burying of glass marbles of 1.5 cm diameter. A mouse was removed from its home cage and allowed to acclimate in the novel cage for 30 min. Following the acclimation period, the mouse was briefly removed from the novel cage, and 20 blue glass marbles were placed in a four-by-five grid on top of the bedding, with each marble spaced 2 cm apart. The mouse was then returned to the novel cage and given 30 additional minutes to explore and interact with the marbles without interference. After this period, the mouse was returned to its home cage, and marble burying was quantified. A score of zero was recorded for unburied marbles, a score of 1 was recorded for a marble that was partially buried, and a score of 2 was recorded for a marble that was buried in its entirety. The marble score was calculated as the sum of the points awarded for the 20 marbles.

Three-chamber sociability and social preference tests. All trials were preceded by a 10 min habituation period, beginning when a mouse was placed in the center chamber of a three-chamber polycarbonate enclosure with 10 cm sliding gates separating the 18 × 23 cm chambers, as used elsewhere in similar experiments (Carter et al., 2011). Both doors were opened, and the mouse was allowed to explore the entirety of the enclosure for 10 min. The mouse was briefly removed from the enclosure to arrange stimuli for the tests. For the object versus social stimulus test (sociability), a nonsocial stimulus (glass marble) and a social stimulus (littermate) were placed within wire cages in the two side chambers, with one stimulus per side chamber. Novel versus known mouse testing was preceded by both the habituation period and the object versus social test. One social stimulus was a littermate from the home cage of the subject mouse, and the other was a novel mouse with which the subject mouse had no previous contact. The placement of these stimuli was randomized. The mouse was then returned to the center chamber of the enclosure and allowed to roam freely without interference for 10 min. This arrangement allowed the subject mouse to freely access either stimuli at any given time, while preventing aggressive behavior from the littermate being used as a social stimulus. During this time, the trial was video recorded and the time spent in prespecified zones of the enclosure was quantified using ANY-maze tracking software (San Diego Instruments). In addition to three zones corresponding to the three chambers of the enclosure, two zones denoted an area surrounding the stimuli to capture the time spent with those stimuli. A blinded observer monitored each trial to manually and separately record the time the subject mouse spent actively interacting with either stimulus, as evident by sniffing. Data were analyzed with a two-way ANOVA, using sociability and genotype as variables in measuring differences in the time spent interacting with social versus nonsocial stimuli. Bonferroni post-test corrections were used, and *p* values observed for the time spent with social versus nonsocial stimulus are indicated in Table 2.

Social reciprocity. This behavioral assay occurred in two trials. In the first trial, each animal was paired with a littermate from the home cage of the subject animal. In the second trial, each animal was paired with a novel mouse with which they had no previous contact. With the exception of animal pairing criteria, both phases were conducted using the same methodology. Two mice were placed in an empty, plastic, square (25 × 25 cm) arena and allowed to explore or interact without interference. This interaction was recorded via an overhead camcorder and scored in real-time by TopScan tracking software (CleverSys). One mouse in each paired trial was marked with a small dot of white-out solution streaked on its fur to aid the TopScan software in differentiating the two mice during the trial. In the event that the software incorrectly mapped the two mouse identities mid-trial, an observer blinded to the genotypes noted the time of the swap and adjusted the data accordingly. All trials were 10 min in length, were recorded in their entirety, and were scored by TopScan for measures of active social contact, passive social contact, and social sniffing. Data were analyzed by a two-way ANOVA using social preference and genotype as variables. Bonferroni post-test corrections were used to correct for multiple testing (see Table 2).

Olfaction test. This behavioral assay occurred in following two trials: nonsocial and social odor detection. In the nonsocial odor detection trial, a cotton swab was briefly dipped in a 10% condensed milk solution and hung from a corner of the home cage of the subject mouse for 2 min. During this time, the mouse was free to explore and interact with the contents of its cage without interference. The amount of time spent within 5 cm of the scented swab or directly interacting with the scented cotton swab was recorded. The social odor detection trial used an identical methodology, with the exception that the cotton swab was dragged through the home cage of a novel mouse directly before being hung in the subject's home cage for 2 min. Data were analyzed with a two-way ANOVA, using odor type and genotype as variables. Bonferroni post-test corrections were used to determine the differences between the time spent with social versus nonsocial stimulus, and *p* values are shown in Table 2.

Immunofluorescence. Mice [7 wild-type (WT) and 4 KI] were perfused with 30 ml of 4% paraformaldehyde (Sigma-Aldrich). Brains were stored in 30% sucrose for 48 h at 4°C and then stereotaxically sectioned every 30 μm on a frozen stage microtome (Leica) and stored in a cryoprotectant solution (30% ethylene glycol, 30% glycerol in PBS). Sections collected between ~4.30 and ~4.90 mm from bregma were defined as midbrain sections containing dorsal raphe nuclei and the periaqueductal gray areas, which were used in this study. Immediately before use, serial sections were washed in Tris-buffered saline (TBS). Slices were treated with Na^+/citrate solution (10 mM tri-sodium citrate dihydrate, pH 6.0 containing 0.05% Tween-20) at 50°C for 5 min. Endogenous peroxidase was quenched by incubating sections in 1% H_2O_2 for 30 min. Slices were blocked with blocking buffer (1× TBS containing 5% goat serum, 1% bovine serum albumin, and 0.25% Triton X-100) for 1 h at room temperature. Primary antibodies were added at a 1:250 dilution in blocking buffer and incubated for 16 h at 4°C. Integrin β3 signal was amplified by preincubating biotinylated anti-rabbit antibody (RRID:AB_2340593) with streptavidin-conjugated horseradish peroxidase (both diluted at 1:500 in blocking buffer) for 15 min at room temperature, followed by incubation with slices for 1 h at room temperature. After washing with 1× TBS, slices were incubated with tyramide solution (TSA Biotin Tyramide Reagent, PerkinElmer) for 10 min. After washing with 1× TBS, fluorescent secondary antibodies (goat anti-mouse-Cy5 (RRID:AB_2338714); goat streptavidin-Cy2 (RRID:AB_2337246); and goat anti-guinea-pig-Cy3 (RRID:AB_2340460); Jackson ImmunoResearch) were applied at a 1:500 concentration for 16 h at room temperature. Slices were washed in 1× TBS and mounted onto slides using Aqua-Poly/Mount (Polysciences).

Confocal and super-resolution structured illumination microscopy. Confocal images were captured using a Zeiss LSM 510 Meta confocal (Zeiss).

Images were acquired using a 40×/1.30 Plan-NEOFLUAR oil-objective with the pinhole set at 1 μm and using a 2.5× digital zoom of the 543 nm laser for Cy-3 (LSM 5 Image Browser, Zeiss). Image analysis for the quantification of fibers was performed as described previously, using ImageJ (Sathyanesan et al., 2012). Super-resolution three-dimensional (3D)-structured illumination microscopy (SIM) Z-series images were acquired for the imaging of 20-μm-thick midbrain slices using a DeltaVision OMX super resolution microscope (GE Healthcare). We used a 65× objective, using an oil refractive index of 1.52 (Prolog Gold). All images were generated from two independent slices of each mouse (number of mice as indicated in figure legends) and were restricted to a maximum of 15 *z*-slices/mouse of the dorsal raphe and adjacent periaqueductal gray area with a 1.5 μm thickness at 0.125 nm resolution (see Fig. 2*A*). Reconstruction of 3D-SIM images was performed using API DeltaVision OMX softWoRx software (GE Healthcare), and two independent researchers, who were blinded to genotype, performed the synapse and axonal measurement and colocalization analysis. Individual puncta or fibers were selected using the region of interest tool and colocalization assessed in the volume selected. Colocalization of two proteins was quantified by the correlation in fluorescence signal in pixels corresponding to 0.1 μm^2, where Pearson correlation coefficients >1.0 and <0.1 were considered positive and negative colocalization, respectively. Initial analysis in WT samples are shown in Figure 2, where we established the mean diameter of $SERT^+$ puncta present in axons and synapses. The size and pattern of punctate structures and positive colocalization of SERT with the presynaptic marker synaptophysin identified synapses, and only synapses measuring 0.9870 ± 0.025 μm in diameter were quantified. Image acquisition and analysis were performed at the Vanderbilt Cell Imaging Shared Resource.

Blood collection, midbrain dissections, and 5-HT and 5-HIAA neurochemistry. Mice were killed by isoflurane overdose followed by cervical dislocation, and blood was collected in sodium citrate via cardiac puncture. Midbrains were dissected by peeling off the cortex and cerebellum to expose the third ventricle and the aqueduct and making two coronal sections at the beginning of the superior colliculus at bregma −3.4 mm and another at the end of the inferior colliculus at bregma −5.2 mm. Samples were analyzed for 5-HT and 5-hydroxyindoleacetic acid (5-HIAA) by high-pressure liquid chromatography (HPLC) using an Antec Scientific Decade II Electrochemical Detector (oxidation, 0.5) operated at 33°C in the Vanderbilt University Brain Institute Neurochemistry Core. Twenty microliter samples of the supernatant from trichloroacetic acid tissue extracts were injected via a Waters 717+ Autosampler onto a Phenomenex Nucleosil C18HPLC column (5 units, 100 A; 150 × 4.60 mm). Amines were eluted with a mobile phase consisting of 89.5% 0.1 M trichloroacetic acid, 10^{-2} M sodium acetate, 10^{-4} M EDTA, and 10.5% methanol, pH 3.8. Solvent was delivered at 0.6 ml/min by using a Waters 515 HPLC Pump.

Synaptoneurosomal uptake and binding measures. Syaptoneurosomes were used in this study to preserve integrin–extracellular matrix (ECM) interactions. Saturation kinetic and competition analyses of 5-HT uptake were performed as previously described (Mazalouskas et al., 2015). Briefly, crude synaptoneurosomal pellets were prepared by homogenization of midbrain tissue (in 0.32 M sucrose with 4 mM HEPES, pH 7.4, containing 0.1 mM $CaCl_2$ and 1.0 mM $MgCl_2$). The resulting synaptoneurosomal pellet was resuspended in uptake buffer (1× Krebs-Ringer Solution, HEPES buffered, containing 1.8 g/L glucose, 100 μM pargyline, and 100 μM ascorbic acid). For saturation analysis, 50 μg of synaptoneurosomes were incubated with increasing concentrations of [^{3}H] 5-HT (12.5–400 nM) for 10 min at 37°C. Uptake was terminated by filtration through polyethyleneimine-coated GF/B Whatman filters using a Brandel Cell Harvester. Filters were washed and immersed in scintillation liquid for 8 h before quantification of accumulated radioactivity by scintillation spectrometry (Beckman Coulter). Counts obtained from the filtered samples were corrected for nonspecific uptake using parallel samples incubated at 37°C with 1.0 μM paroxetine. For dopamine uptake experiments, striatal synaptosomes were incubated with increasing concentrations of [^{3}H] dopamine (25–800 nM) and 100 μM cocaine was used to correct for nonspecific uptake.

For binding of [^{3}H] citalopram to purified presynaptic membranes to calculate B_{max} values, synaptoneurosomal pellets were hypotonically lysed in 10 volumes of H_2O, equilibrated to 50 mM Tris, pH 7.4, and rotated end-over-end for 20 min at 4°C. Plasma membranes were pelleted via centrifugation at 15,000 × *g* for 25 min at 4°C and resuspended in binding buffer (50 mM Tris, pH 7.4, 120 mM NaCl, and 5 mM $MgCl_2$). Purified membranes (45 μg) were preincubated in the absence or presence of 1.0 μM paroxetine for 30 min at 4°C, followed by incubation with increasing concentrations of [^{3}H] citalopram (6.25–400 nM) for 20 min at 4°C. Binding was terminated by filtration as described above.

For studies examining the effects of kinase inhibitors on SERT-mediated [^{3}H] 5-HT uptake in WT and KI samples, synaptoneurosomes (50 μg) were incubated with 100 nM SKI-606 or PF-573228 for 10 min at 37°C in the presence or absence of 1.0 μM paroxetine. After this incubation period, increasing concentrations of [^{3}H] 5-HT (12.5–400 nM) were added, and samples were incubated for 10 min at 37°C. Termination of uptake and filtration was performed as described above.

Western blotting and coimmunoprecipitation. Crude synaptoneurosomes were lysed in 1% Triton X-100 in PBS (containing protease and phosphatase inhibitors) and clarified by centrifugation at 13,000 × *g* for 10 min at 4°C. Lysates were collected for input (50 μg), and 800 μg of protein extract was incubated with integrin β3 antibody (2C9.G2 hamster anti-mouse β3, BioLegend) covalently attached to protein A magnetic beads (Dynabeads, Life Technologies/Invitrogen) for 1 h at 4°C with end-over-end rotation. Beads were isolated magnetically and washed with lysis buffer. Coimmunoprecipitated proteins were eluted with 1× Laemmli sample buffer and either boiled for 5 min or heated to 37°C for 10 min. Lysates and immunoprecipitates were resolved on Tris-Glycine polyacrylamide gels (Life Technologies) and transferred to Immobilon-P 0.45 μm PVDF (Millipore) to perform Western blot analysis. Proteins were detected by chemiluminescence and exposed to Hyperfilm through multiple exposures to ensure linear distribution of the signal. Films were scanned, and band densities were established using ImageJ software (National Institutes of Health).

Data analyses. All data were analyzed using GraphPad Prism software (Prism 6, GraphPad Software). Imaging analyses took into consideration the number of events (axons, synapses, or slices), which are reported in the figure legends. The number of biological replicates (number of animals, *N*) is indicated in the Results section. The reported data for imaging studies originates from the initial analysis by the first experimenter. However, a second blinded experimenter also quantified the images, and no significant differences were observed between the means of the first and second experimenter. The minimum number of technical replicates for all experiments, which is defined by the number of cohorts of animals, is three. The Michaelis–Menten curve fit as a function of ligand concentration revealed K_m and V_{max} values in uptake and K_d and B_{max} in binding experiments, respectively. Statistical analysis of individual representative curves was performed by multiple *t* testing using the Holm–Sidak method with $\alpha < 0.05$. Tests where two independent variables were assayed were analyzed using a two-way ANOVA and Bonferroni corrections for multiple testing between categories (indicated in figure legends). Remaining data were analyzed using an unequal variance Welch *t* test, $\alpha<0.05$. Raw data are presented, with the means ± SEMs shown as line and whiskers.

Results

The human Pro33 variant is associated with attention-deficit hyperactivity disorder and ASD in males, but not females

We used the systematic approach of a PheWAS to identify novel neuropsychiatric phenotypes associated with the rs5918 Leu33Pro coding polymorphism (Denny et al., 2010, 2011, 2013). We leveraged extant genotyping data from a large DNA databank, termed BioVU, composed of deidentified patient samples and corresponding electronic medical record-derived phenotype data from Vanderbilt University Medical Center (Roden et al., 2008). The genotype data, including for rs5918, was obtained from the Illumina HumanExome Chip and included 11,419 males and 13,609 females, adjusted for age and stratified by sex. The pooled minor allele frequency (C allele) across all racial groups is 0.1494 in the BioVU Exome Chip stratified as follows: CC, 2%; CT, 25%;

Table 1. Human PheWAS identifies neuropsychiatric disorders associated with the integrin β3 coding polymorphism Leu33Pro (rs5918)

	Adult females				Adult males			
Psychiatric disorder	Case patients	Control subjects	OR	*p* value	Case patients	Control subjects	OR	*p* value
ADHD	*54*	*13,561*	*1.24*	*0.3745*	*46*	*11,371*	*2.09*	*0.0014*
Pervasive developmental disorders (ASDs)	*66*	*13,561*	*1.21*	*0.4067*	*61*	*11,371*	*1.91*	*0.0018*
Schizophrenia	47	8478	0.97	0.9260	29	8404	0.39	0.0683
Suicidal ideation or attempt	48	8478	1.18	0.5325	55	8404	0.58	0.0872
Antisocial/borderline personality disorder	39	8478	0.92	0.7924	14	8404	0.19	0.1061
Suicidal ideation	26	8478	1.53	0.1970	30	8404	0.48	0.1108
Major depressive disorder	499	8478	1.08	0.3699	273	8404	1.18	0.1328
Psychogenic and somatoform disorders	92	8478	0.84	0.4269	21	8404	0.41	0.1331
Agoraphobia, social phobia, and panic disorder	121	8478	1.17	0.3423	54	8404	0.66	0.1717
Transient alteration of awareness	48	11202	0.81	0.4855	31	9205	0.58	0.1989
Obsessive-compulsive disorders	30	8478	0.90	0.7733	17	8404	1.58	0.2542
Personality disorders	66	8478	0.86	0.5331	32	8404	0.64	0.2689
Generalized anxiety disorder	189	8478	0.84	0.2440	101	8404	1.22	0.2700
Other specified nonpsychotic and/or transient mental disorders	612	11,202	1.04	0.6052	630	9205	0.92	0.3314
Posttraumatic stress disorder	134	8478	1.03	0.8740	55	8404	1.24	0.3703
Eating disorder	35	8478	1.50	0.1554	6	8404	1.72	0.4136
Anxiety, phobic and dissociative disorders	1968	8478	1.00	0.9188	950	8404	0.95	0.4144
Anxiety disorder	1559	8478	0.95	0.3228	731	8404	0.95	0.4749
Aphasia/speech disturbance	242	11,202	1.18	0.1526	237	9205	0.91	0.4904
Bipolar	*226*	*8478*	*0.74*	*0.0350*	152	8404	1.10	0.5250
Dysthymic disorder	419	8478	1.10	0.3009	177	8404	0.93	0.6514
Mental retardation	48	13,561	0.87	0.6415	48	11,371	0.92	0.7791
Depression	2370	8478	1.04	0.3252	1276	8404	0.99	0.8735
Mood disorders	2565	8478	1.04	0.4239	1435	8404	1.00	0.9278
Conduct disorders	36	13,561	0.92	0.8067	42	11,371	0.99	0.9675

Odds ratios (ORs) are reported as increased risk for the rare allele Pro33. *p* values are presented as raw, uncorrected values. Italics is used to indicate disorders with statistically significant associations.

and TT, 73%. We tested for association across 25 PheWAS codes corresponding to psychiatric conditions. Two associations surpassed a Bonferroni correction threshold (0.05/25 = 0.002) in males, but not in females (Table 1): attention-deficit hyperactivity disorder (ADHD; males: OR = 2.09; 95% CI = 1.33–3.28; females: OR = 1.24; 95% CI = 0.77–2.02) and ASD (males: OR = 1.91; 95% CI = 1.27–2.86; females: OR = 1.21; 95% CI = 0.78–1.88).

KI mice display alterations in behaviors

As loss of integrin β3 expression has been implicated in the regulation of behaviors associated with social communication (Carter et al., 2011), we examined the behavior of male KI mice in a battery of tests measuring anxiety, behavioral despair, repetitive, and social behaviors (Table 2; Brocco et al., 2002; Cryan and Holmes, 2005; Cryan et al., 2005a,b; Thakker et al., 2005). The open field test revealed that, although both genotypes traveled similar distances in a familiar environment, exploratory activity in a novel environment was significantly reduced in KI mice when compared with WT mice. When subjected to an elevated zero maze, KI mice displayed similar locomotor activity and spent the same time as WT littermates exploring the arms of the maze, but KI mice entered the open quadrants significantly less often than WT mice. We obtained discordant genotype effects in behavioral despair tests, where KI mice demonstrated a greater immobility time during the tail suspension test but no differences in the forced swim test. To measure repetitive behavior, we used the marble-burying test, which revealed that KI mice bury fewer marbles than WT littermates. Two different tests were used to measure social behaviors in KI mice. The three-chamber test was used to measure the preference of mice for a novel social cue compared with an object or a known social cue. The object versus mouse test measures sociability, which was similar between WT and KI mice, as both genotypes spent more time sniffing the social cue (mouse). KI mice displayed a deficit in social preference as they spent the same amount of time interacting with a known mouse and a novel mouse, while WT mice spent significantly more time interacting with novel mice. We then performed two different social reciprocity tests to identify qualitative alterations in social interactions in KI mice. In the first, we observed the interaction between two littermates (genotypes were randomized) to assess the initiation of contact and sniffing in each mouse. KI mice initiated a smaller number of contacts and spent less time interacting with their littermate. During this interaction, KI mice also initiated a smaller number of sniffing events and spent less time sniffing when compared with WT littermates. We then exposed each mouse to a novel male mouse (genotypes randomized). In this paradigm, KI mice also initiated fewer contacts and spent less time within each contact, but their sniffing behavior was comparable to those observed in WT mice. As the social tests demand appropriate identification of olfactory cues, we exposed mice to two olfactory stimuli, a nonsocial stimulus (banana extract) and a social stimulus (urine). Both genotypes performed equally in this test, indicating that the social deficits observed in KI mice do not result from alterations in the recognition of olfactory stimuli.

Altered 5-HT neurochemistry and anatomy in KI mice

The association of the human Pro33 integrin β3 variant with elevated blood 5-HT levels prompted us to examine peripheral and central levels of 5-HT and its metabolite 5-HIAA in KI mice. HPLC studies of blood samples revealed elevated levels of 5-HT and decreased 5-HT turnover, as determined by an increase in the 5-HT/5-HIAA ratio in whole blood of KI mice (Fig. 1*A*; 5-HT: $p = 0.04$; 5-HT/5-HIAA ratio: $p = 0.02$; WT mice: $N = 11$; KI mice: $N = 8$). In the midbrain and hippocampus, no genotype differences were observed in 5-HT levels, although 5-HT turnover was decreased (Fig. 1*B*: 5-HT/5-HIAA ratio, $p = 0.03$; WT

Table 2. Behavioral characterization of male KI mice

	WT				KI				
Behavior	Mean		SEM	*N*	Mean		SEM	*N*	*p* value
Open field									
Ambulatory distance-acclimated	2195.00	±	252.60	13	1943.00	±	322.80	8	0.547
Ambulatory distance-novel	*3964.47*	±	*456.82*	*13*	*2480.14*	±	*103.00*	*8*	*0.017*
Stereotypy	5750.08	±	223.42	13	5244.63	±	112.50	8	0.258
% Time in the center of the arena	10.57	±	5.10	13	18.90	±	2.87	8	0.696
Elevated zero maze									
Distance traveled (m)	7.66	±	0.69	15	5.85	±	0.23	8	0.090
Number of entries in Open	*13.13*	±	*1.46*	*15*	*9.13*	±	*0.36*	*8*	*0.025*
% Time in the closed arm	34.21	±	2.48	15	38.15	±	4.41	8	0.451
Forced swim test									
Latency to immobility (s)	54.87	±	13.74	15	57.50	±	12.62	8	0.889
Immobility in the last 4 min (s)	87.21	±	10.12	15	91.75	±	19.17	8	0.838
Tail suspension test immobility (s)	*249.60*	±	*12.90*	*8*	*314.50*	±	*10.00*	*5*	*0.002*
Marble burying score	26.50	±	2.32	6	18.50	±	1.67	6	*0.021*
Social reciprocity-novel mouse									
Number of contacts	*11.00*	±	*2.43*	*10*	*4.78*	±	*1.52*	*9*	*0.047*
Duration of active contact	*55.48*	±	*11.62*	*10*	*20.96*	±	*7.65*	*9*	*0.025*
Number of sniffing events	15.50	±	3.65	10	8.22	±	2.58	9	0.124
Time spent sniffing	6.72	±	1.60	10	3.91	±	1.13	9	0.172
Social reciprocity-littermate									
Number of contacts	*10.38*	±	*1.37*	*13*	*5.90*	±	*0.91*	*10*	*0.013*
Duration of active contact	*37.21*	±	*6.15*	*13*	*20.63*	±	*4.59*	*10*	*0.042*
Number of sniffing events	*13.69*	±	*1.76*	*13*	*7.20*	±	*1.35*	*10*	*0.008*
Time spent sniffing	*5.28*	±	*0.75*	*13*	*2.61*	±	*0.50*	*10*	*0.008*
	Mean 1	Mean 2			Mean 1	Mean 2			
3-Chamber									
Object vs social	38.02	78.12	6		22.05	64.70	6		WT = 0.002, KI = 0.001
Known mouse vs novel mouse	*34.78*	*78.38*	*5*		*27.23*	*58.32*	*6*		*WT = 0.015, KI = 0.051*
Olfactory test									
Object vs social	23.10	52.63	6		21.72	37.48	6		WT = 0.0006, KI = 0.031

Behaviors that show a significant difference between genotypes are shown in italics ($p < 0.05$). All data was analyzed using unpaired Student's *t* test with Welch's correction, except in social tests, where Bonferroni-corrected post-tests are shown.

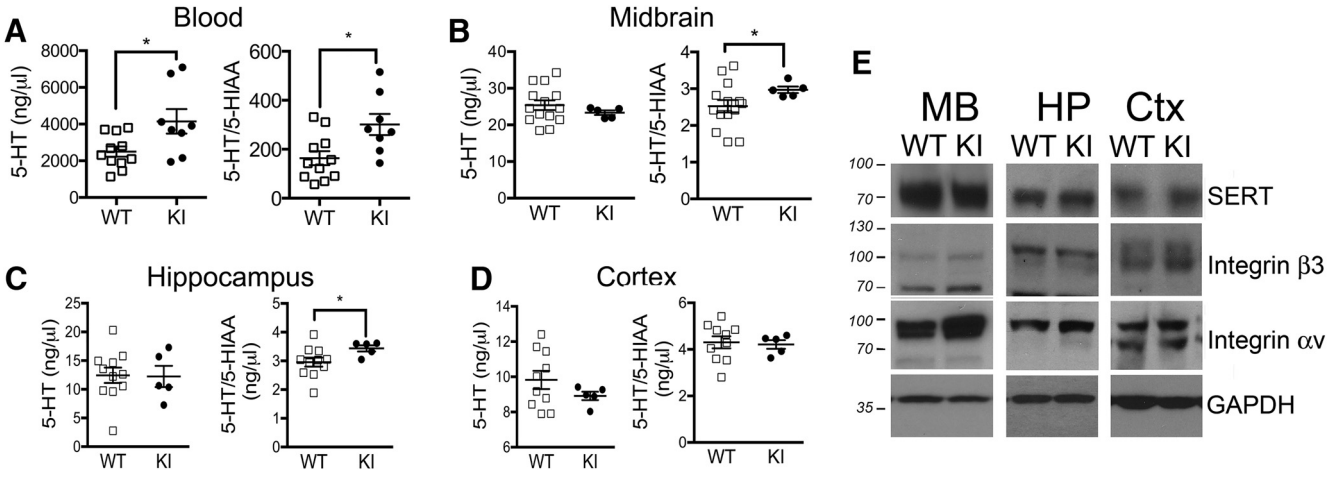

Figure 1. Altered 5-HT neurochemistry in integrin β3 KI mice. ***A–D***, HPLC analyses of 5-HT and 5-HT turnover (5-HT/5-HIAA ratio) in whole blood and isolated regions of the mouse CNS. ***A–D***, Blood was extracted by cardiac puncture for measurement of whole-blood 5-HT and 5-HIAA (5-HIAA levels: WT mice, 18.36 ± 2.76; KI, 13.44 ± 2.11, $p = 0.17$; 5-HT, $p = 0.04$; 5-HT/5-HIAA ratio, $p = 0.02$; WT mice, $N = 11$; KI mice, $N = 8$; ***A***), and 5-HT and 5-HT turnover for midbrain (5-HIAA levels: WT mice, 10.67 ± 0.83; KI mice, 7.87 ± 0.24; $p = 0.005$; 5-HT/5-HIAA ratio: $p = 0.03$; WT mice, $N = 14$; KI mice, $N = 5$; ***B***), hippocampus (5-HIAA levels: WT mice, 4.37 ± 0.53; KI mice, 4.26 ± 0.38; $p = 0.35$; 5-HT/5-HIAA ratio: $p = 0.03$; WT mice, $N = 11$; KI mice, $N = 5$; ***C***), and cortex (5-HIAA levels: WT mice, 2.34 ± 0.16; KI mice, 2.13 ± 0.12; $p = 0.39$; WT mice, $N = 10$; KI mice, $N = 5$; ***D***). ***E***, Representative Western blot of synaptosomes isolated from midbrain, hippocampus, and cortices of KI and WT mice. Samples were exposed to anti-SERT antibodies (SERT: WT mice, $N = 4$; KI mice, $N = 3$), integrin β3 (WT mice, $N = 5$; KI mice, $N = 6$), integrin αv (WT mice, $N = 6$; KI mice, $N = 4$) and GAPDH (WT mice, $N = 5$; KI mice, $N = 6$). All data were analyzed using an unpaired *t* test with Welch's correction. *$p < 0.05$.

mice, $N = 14$; KI mice, $N = 5$; Fig. 1*C*: 5-HT/5-HIAA ratio, $p = 0.03$. WT mice, $N = 11$; KI mice, $N = 5$). No changes in 5-HT neurochemistry were observed in the cortices of KI mice when compared with wild-type littermates (Fig. 2*D*; WT mice, $N = 10$; KI mice, $N = 5$). Western blot analysis of the synaptosomes isolated from midbrain, hippocampus, and cortices of KI and WT mice shows no changes in the expression levels of either SERT (WT mice, $N = 4$; KI mice, $N = 3$), or the β3 (WT mice, $N = 5$; KI mice, $N = 6$) and αv (WT mice, $N = 6$; KI mice, $N = 4$) subunits of the integrin αvβ3 receptor (Fig. 1*E*).

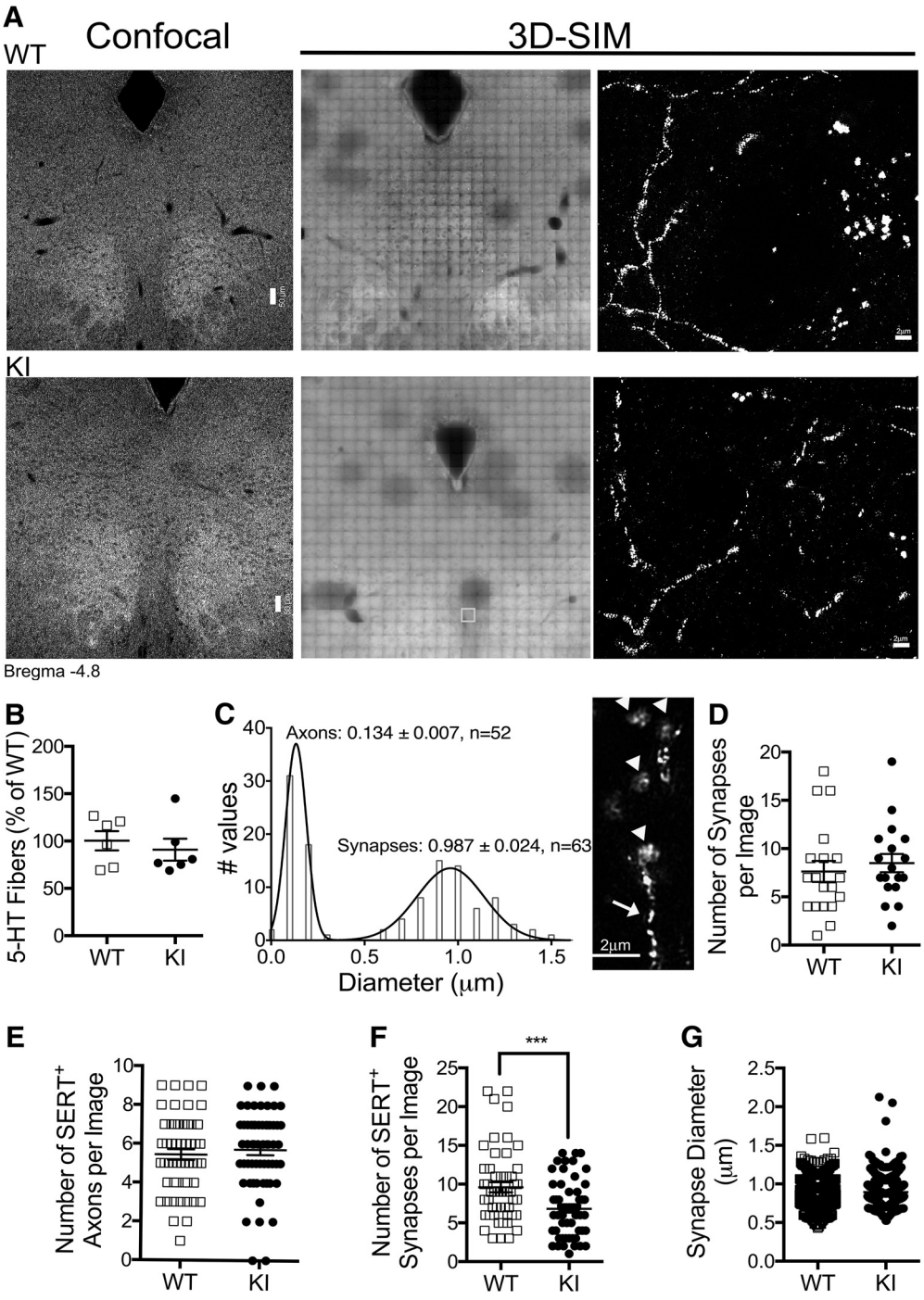

Figure 2. Immunofluorescence studies of midbrains isolated from integrin β3 KI mice. Serial slices of midbrains (distance from bregma, −4.4 to −4.9 mm) were stained with anti-SERT and anti-synaptophysin antibodies for identification of 5-HT fibers and synapses. ***A***, Representative confocal (left panels; scale bar, 50 μm), OMX spiral mosaic (middle), and 3D-SIM (left; scale bar, 2 μm) microscopic images showing SERT staining. The same WT (top) and KI (bottom) slices were imaged in confocal and OMX microscopes (compare left and middle panels). Dorsal raphe regions sampled by 3D-SIM can be seen in middle panels as quenched areas. ***B***, SERT-expressing fibers were quantified by optical density analysis of confocal images ($N = 6$ mice/genotype). ***C***, Frequency distribution of the diameter of SERT-expressing puncta obtained by 3D-SIM. Means and SEM in micrometers are indicated in the histogram and *N* values represent the total number of events obtained from multiple images ($N = 4$ WT mice). Small puncta (axonal vesicles) are indicated by arrows and large puncta (synapses) by arrowheads in representative figure in the right. ***D***, Quantification of the number of puncta ~1 μm in diameter expressing synaptophysin from WT and KI images (WT, 19 images; KI, 18 images; $N = 3$ mice per genotype). ***E***, Quantification of the number of axons expressing SERT in images obtained from WT and KI slices (WT, 52 images; KI, 59 images; $N = 3$ mice/genotype). ***F***, Quantification of the number of puncta coexpressing SERT and synaptophysin (WT, 52 images; KI, 56 images; $N = 3$ mice/genotype; $p = 0.001$). ***G***, Quantification of the diameter of synapses expressing SERT and synaptophysin (WT, 496 synapses; KI, 377 synapses; $N = 3$ mice/genotype). All data were analyzed using unpaired *t* test with Welch's correction. ***$p = 0.001$.

Multiple integrins are involved in axonal pathfinding and targeting during CNS development and, therefore, may influence the migration of 5-HT axons to terminal fields (Clegg et al., 2003; Blaess et al., 2004; Gu et al., 2009; Murase et al., 2011). To examine fiber density in the midbrains of WT and KI mice, we stained brain sections with SERT antibodies. Confocal analysis of slices revealed a similar density of SERT-expressing fibers in the dorsal raphe and adjacent periaqueductal gray areas (distance from

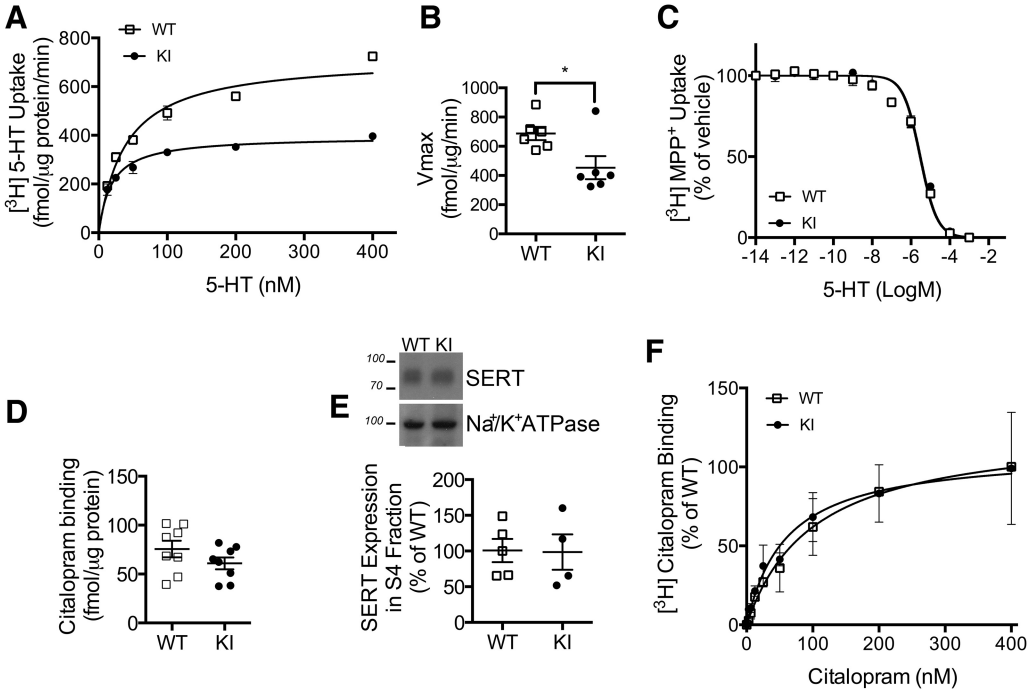

Figure 3. SERT function is altered in KI mice. ***A***, Representative kinetic saturation curves of SERT-mediated [^{3}H] 5-HT uptake in midbrain synaptoneurosomes from WT (□) and KI (●) mice. ***B***, Analysis of maximum SERT-mediated 5-HT transport velocity (V_{max}) from pooled kinetic saturation experiments (unpaired *t* test with Welch's correction, $p = 0.033$; $N = 6$ per genotype). ***C***, 5-HT competition of [^{3}H] MPP$^+$ (1-methyl-4-phenylpyridinium) uptake. $N = 4$ per genotype. ***D***, [^{3}H] citalopram binding to intact synaptoneurosomes. $N = 8$ per genotype. ***E***, Plasma membrane fractions from WT and KI synaptoneurosomes were analyzed by Western blotting for levels of SERT and Na$^+$/K$^+$ ATPase (loading control). Representative blots (***E***, top) and quantification for $N = 5$ mice per genotype (***E***, bottom) are shown. ***F***, Analysis of saturation [^{3}H] citalopram binding to purified synaptoneurosome plasma membranes. $N = 3$ per genotype. *$p < 0.05$.

bregma, −4.4 to −4.9 mm; Fig. 2*A*, left panels, *B*; $N = 6$ per genotype). To better assess changes in fine anatomy and to differentiate axons and synapses, we used super-resolution 3D-SIM techniques (Mazalouskas et al., 2015). This technique allows the imaging of the same slices in confocal and OMX microscopes, as shown in Figure 2*A*. The image field of each OMX microscope is bleached and reconstructed digitally, revealing a series of SERT-expressing fibers and synapses. To define those two populations, we first measured the diameter of SERT-expressing puncta and observed the following two distinct populations: a population measuring ~0.15 μm (Fig. 2*C*, arrows) and a population measuring ~1.0 μm (Fig. 2*C*, arrowheads), which were defined as axonal vesicles and synapses, respectively (Fig. 2*C*; $N = 4$ WT mice). We then counted the number of synapses expressing synaptophysin (Fig. 2*D*), axons (Fig. 2*E*), and synapses expressing SERT (Fig. 2*F*) in images obtained from WT and KI slices ($N = 3$ mice/genotype). We observed an ~30% reduction in the number of synapses expressing SERT in KI slices (Fig. 2*F*; $p = 0.001$; $N = 3$ mice/genotype), although no differences were observed in the total number of synapses or SERT$^+$ fibers. SERT$^+$ synapses also had comparable diameter in WT and KI samples (Fig. 2*G*; $N = 3$ mice/genotype). Together, we have observed small but significant reductions in serotonergic synapses and 5-HT turnover in the midbrains of mice expressing the Pro32Pro33 integrin, suggesting that constitutive activation of integrin αvβ3 alters both the homeostasis and structure of the 5-HT system.

Synaptic SERT function is impaired in KI mice

Initial studies associated genetic variation in *Itgb3* with changes in 5-HT homeostasis via the physical and functional interaction of the integrin β3 protein with SERTs (Carneiro et al., 2008; Whyte et al., 2014; Mazalouskas et al., 2015). To determine whether the Pro32Pro33 mutation in integrin β3 also alters midbrain 5-HT uptake, we measured synaptic SERT activity in WT and KI mice (Fig. 3). Saturation 5-HT uptake assays using midbrain synaptoneurosomes demonstrated decreased SERT activity in KI mice compared with WT mice. Representative 5-HT saturation curves are shown in Figure 3*A*. There was no significant difference in transporter affinity (K_m) for 5-HT between phenotypes (WT: 34.4 ± 4.7 nM, $N = 6$; KI: 30.7 ± 6.7 nM, $N = 6$); however, we observed a 40% reduction in transporter capacity (V_{max}) in KI synaptoneurosomes (Fig. 3*B*; $p = 0.03$; $N = 6$ per genotype). Dopamine transporter-mediated uptake of dopamine in samples isolated from the striatum, the major organizing center for the dopaminergic system (Joel and Weiner, 2000), was not affected by the Pro32Pro33 mutation (K_m: WT: 83.6 ± 10.2 nM; $N = 3$; KI: 64.6 ± 36.52 nM; $N = 3$; V_{max}: WT: 117.4 ± 4.2%; $N = 3$; KI: 99.5 ± 15.4%; $N = 3$). Thus, the observed Pro32Pro33 integrin-β3-driven changes in midbrain 5-HT uptake do not result from a general dysfunction in monoamine uptake.

The observed decrease in SERT-mediated 5-HT uptake in KI mice could result from changes in 5-HT potency, SERT availability, or SERT catalytic activity. 5-HT potency was unaltered in KI mice, as measured by an MPP$^+$ competition assay (Fig. 3*C*; $N = 4$ mice/genotype), and the binding of ^{3}[H] citalopram to intact synaptosomes indicates that there are no changes in SERT protein levels at synaptic terminals (Fig. 3*D*; $N = 8$ per genotype). Analysis of purified presynaptic membranes (Phillips et al., 2001) from WT and KI midbrains did not reveal any changes in surface levels of SERT protein by Western blot (Fig. 3*E*; WT mice, $N = 5$; KI mice, $N = 4$) or in saturation [^{3}H] citalopram binding to purified membranes (Fig. 3*F*; $N = 5$ per genotype). These findings indicate that the changes in SERT function in KI mice were likely a result of decreased catalytic activity, where the transport

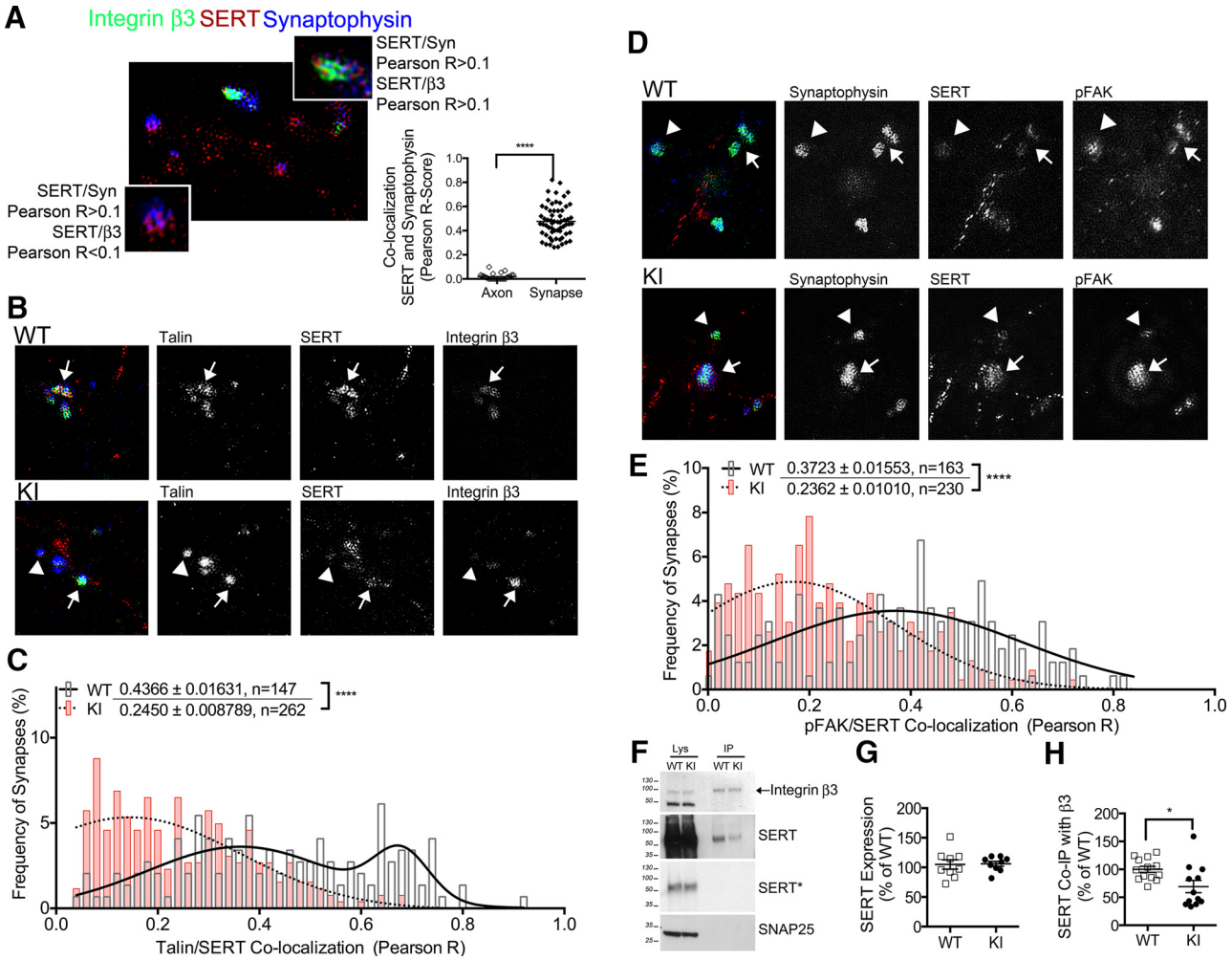

Figure 4. SERT association with integrin signaling complexes is decreased in KI mice. ***A***, SIM depicting colocalization of synaptophysin and SERT in integrin $\beta3$-positive (top inset) and $\beta3$-negative (bottom inset) WT midbrain synapses. Inset graph, Proof-of-principle colocalization analysis between SERT and synaptophysin showing significant increases in Pearson *R* score in synapses (diameter, ~1 μm), when compared with axons. $N = 26$ axons; $N = 63$ synapses. Images were obtained from four WT mice. ***B***, SIM images depicting colocalization of talin (blue), SERT (red), and integrin $\beta3$ (green) in WT (top) and KI (bottom) midbrain synapses. Arrow, colocalization of talin and SERT. Arrowhead, Talin-containing synapse absent of SERT. ***C***, Frequency distribution of Pearson's *R* scores for synapses positive for SERT/talin colocalization (data presented on the top of graph as the mean ± SEM; unpaired *t* test with Welch's correction, $p < 0.0001$; number of synapses: WT, $N = 147$; KI, $N = 262$). ***D***, SIM images depicting colocalization of synaptophysin (green), SERT (red), and pFAK(Y397; blue) in WT (top) and KI (bottom) midbrain synapses. Arrow, Colocalization of pFAK and SERT. Arrowhead, pFAK-containing synapse absent of SERT. ***E***, Frequency distribution of Pearson's *R* scores for synapses positive for SERT/pFAK colocalization (data presented on the top of graph as the mean ± SEM; unpaired *t* test with Welch's correction, $p < 0.0001$; number of synapses: WT, $N = 147$; KI, $N = 262$). For ***B–E***: 3 animals/genotype. ***F–H***, Lysates (Lys) and integrin $\beta3$ immunoprecipitates (IPs) from WT and KI midbrain synaptoneurosomes were analyzed by Western blotting and densitometry for levels of integrin $\beta3$ and SERT. SNAP25 levels were determined as a loading control. Representative blots are shown in ***F***, in which a lower exposure for SERT ("SERT*") was necessary to clearly depict lysate SERT levels. ***G***, Quantification of synaptosomal protein lysates (50 μg) for SERT expression in WT and KI (N = 9 per genotype). ***H***, Quantification of coimmunoprecipitated SERT from 12 biological replicates (WT/KI pairs), $p = 0.023$. For ***G*** and ***H***: raw densitometry values were normalized to the average of WT values for each technical replicate. Number of technical replicates, 3. All data were analyzed using unpaired *t* test models with Welch's correction: *$p < 0.05$; ****$p < 0.0001$.

of each 5-HT molecule (V_{max}/B_{max}) is reduced by 40% in KI synapses.

Decreased association of SERT with integrin adhesion complexes in KI synapses

Our laboratory demonstrated that SERT and $\alpha v\beta3$ receptors colocalize in midbrain presynaptic terminals (Mazalouskas et al., 2015), suggesting that SERT is localized to multiprotein complexes coordinated by integrin $\alpha v\beta3$ in midbrain synapses. Previous studies suggest that in platelets, the association of SERT with activated $\alpha IIb\beta3$ integrins, and its localization to adhesion complexes, are correlated with increased uptake activity (Carneiro et al., 2008). Here we used 3D-SIM (Allen et al., 2014; Mazalouskas et al., 2015), an unbiased approach for identifying protein colocalization, to quantify the colocalization of SERT and focal adhesion markers in WT and KI midbrain synapses. Colocalization was quantified by the correlation in fluorescence signal in pixels corresponding to 0.1 μm^2, where Pearson correlation coefficients >0.1 and <0.1 were considered to be positive and negative colocalization, respectively. This is demonstrated in Figure 4*A*, in which a WT midbrain slice stained for integrin $\beta3$, SERT, and synaptophysin identified both integrin $\beta3$-positive (Fig. 4*A*, top, inset) and $\beta3$-negative (Fig. 4*A*, bottom, inset) synapses. As a proof of principle, we calculated average Pearson *R* scores for colocalization between SERT and synaptophysin, a presynaptic marker, in synapses and axons, and observed that Pearson correlation scores are significantly higher (Pearson $R = 0.476 \pm 0.017$) in synapses than axons (Pearson $R = 0.019 \pm 0.004$; $N = 4$ WT mice). We quantified the synaptic colocalization of SERT and focal adhesion markers talin (Fig. 4*B*,*C*) and

Table 3. Protein colocalization in WT and KI Synapses

	Pearson $R > 0.1$ (%)		
Protein markers	WT	KI	χ^2
SERT and Talin	*83*	*49*	$\chi^2, df = 25.76, 1$ $z = 5.075, p < 0.0001$
SERT and pFAK	*88*	*74*	$\chi^2, df = 6.368, 1$ $z = 2.523, p = 0.0116$
pFAK and Synaptophysin	*76*	*88*	$\chi^2, df = 4.878, 1$ $z = 2.209, p = 0.0272$

Significant genotype differences in the number of synapses are indicated in italics. Structured illumination microscopy of WT and KI midbrain slices was used to quantify the colocalization of the listed proteins within SERT-positive synapses. The χ^2 test was used to compare the proportion of synapses with a Pearson score >0.1 to the total number of synapses (shown here as percentages) between genotypes.

pFAK (Fig. 4*D*,*E*). In WT midbrain synapses, talin was present in 83% of SERT-positive synapses (as measured by an $R > 0.1$ Pearson correlation score), while only 49% of SERT-positive KI synapses contained talin (Table 3; $N = 3$ mice/genotype). Within those synapses coexpressing SERT and talin, there was a significant reduction in colocalization between SERT and talin in KI mice, as revealed by the difference in mean Pearson correlation coefficients, compared with WT mice (Fig. 4*C*; $p < 0.0001$). We also observed that a population of synapses with high correlation scores (>0.6) is absent from KI samples. In WT midbrain synapses, pFAK was present in 87% of SERT-containing synapses, whereas only 74% of SERT-positive KI synapses contained pFAK (Table 3; $N = 3$ mice/genotype). Within those synapses, we also observed a significant reduction in colocalization between pFAK and SERT in KI synapses, as revealed by the difference in mean Pearson correlation coefficients (Fig. 4*E*), suggesting that constitutive activation of integrin β3 decreases the association of SERT with integrin adhesion complexes. Moreover, we observed an increase in the colocalization of pFAK and synaptophysin in SERT-positive synapses in KI midbrains (Table 3), indicating that synaptic integrin signaling is elevated by the Pro32Pro33 mutation.

To determine whether the Pro32Pro33 mutation affects the αvβ3 receptor–SERT interaction in midbrain synapses, we performed coimmunoprecipitation experiments. Western blot analysis of midbrain synaptoneurosomal lysates confirmed similar expression of the integrin β3 subunit (~100 kDa) and SERT proteins in both genotypes (Fig. 4*F*; representative blot of $N = 12$). Equal amounts of the integrin β3 subunit were immunoprecipitated from WT and KI starting material; however, the amount of SERT coimmunoprecipitated with integrin β3 was reduced by 30% (Fig. 4*H*; WT mice, $N = 13$; KI mice, $N = 12$). Quantification of total and integrin β3-associated SERT levels from 12 separate experiments are shown in Figure 5, *G* and *H*, respectively. These results demonstrate that the Pro32Pro33 mutation in integrin β3 is sufficient to reduce the interaction between SERT and integrin αvβ3–protein complexes in midbrain synapses.

Rescue of synaptic SERT function by inhibition of FAK

Integrin activation promotes the formation of signaling complexes and the initiation of signaling via specific tyrosine kinases, such as Src and FAK, to regulate a variety of cellular functions (Cabodi et al., 2010). We previously found that platelets from KI mice have elevated Src activity (Oliver et al., 2014), and multiple studies from other groups have identified alterations in FAK activity in platelets and cells that express the human Pro33 integrin β3 (Vijayan et al., 2003b; Carneiro et al., 2008). Given our data demonstrating suppressed SERT function in KI synapses that contain the Pro32Pro33 integrin β3 subunit, we hypothesized that increased signaling from integrin-regulated tyrosine kinase drives this phenomenon. To identify contributing kinases, we monitored SERT-mediated uptake of radiolabeled 5-HT in midbrain synaptoneurosomes in the presence of small-molecule inhibitors that target Src or FAK. Representative saturation curves following Src or FAK inhibition are shown in Figure 5, *A* and *D*, respectively, and V_{max} plots from pooled data are shown in Figure 5, *B* and *E*, respectively. Treatment with the dual Src/Abl tyrosine kinase inhibitor SKI-606 blocked 5-HT uptake in WT synaptoneurosomes but had no effect on SERT activity in KI synaptoneurosomes (Fig. 5*B*; vehicle, $N = 5$ per genotype; SKI-606, $N = 3$ per genotype. Bonferroni-corrected post-tests: $\text{vehicle}_{\text{WT vs KI}}$, $p = 0.012$; $\text{WT}_{\text{vehicle vs SKI-606}}$, $p = 0.013$). However, the inhibition of FAK with PF-573228, while not affecting SERT function in WT synaptoneurosomes over a range of concentrations (Fig. 5*C*; $N = 8$), completely restored 5-HT uptake in KI synaptoneurosomes (Fig. 5*E*; vehicle, $N = 7$ per genotype; PF-573228, $N = 5$ per genotype; Bonferroni-corrected post-tests: $\text{vehicle}_{\text{WT vs KI}}$, $p = 0.002$; $\text{KI}_{\text{vehicle vs PF-573228}}$, $p = 0.028$). This suggests that increased FAK signaling downstream of integrin β3 subunits containing the Pro32Pro33 mutation is driving the suppression of SERT V_{max} observed in the midbrain synaptoneurosomes of KI mice.

Discussion

Integrins are transmembrane proteins that interact with the ECM to link the extracellular environment to the intracellular cytoskeleton. Integrin/ECM engagement initiates signaling cascades that drive a variety of cellular functions, including adhesion, motility, and transcription (Hynes, 2002). Of several lines of evidence linking *ITGB3* with the 5-HT system, the role of the coding polymorphism Leu33Pro (rs5918, PI^{A2}) is perhaps the best characterized (Weiss et al., 2006a,b; Coutinho et al., 2007; Ma et al., 2010; Napolioni et al., 2011). This polymorphism in the integrin β3 subunit produces a hyperactive αvβ3 receptor and is associated with elevated whole-blood 5-HT levels and ASD in multiple studies (Coutinho et al., 2007; Napolioni et al., 2011; Singh et al., 2013) and was validated here using an unbiased approach (Denny et al., 2013). We also observed a significant male-specific association of the Pro33 allele with ADHD risk, reinforcing a role of cell adhesion receptors on attention deficit both in human and mouse (Kent et al., 2008; Lasky-Su et al., 2008; Arias-Vásquez et al., 2011; Rivero et al., 2015; Salatino-Oliveira et al., 2015; Tzanoulinou et al., 2016). The genetic studies also may indicate a common mechanism causing 5-HT dysfunction, hyperactivity (Banerjee and Nandagopal, 2015; Whitney et al., 2016), and ASD (Muller et al., 2016) and thus prompted us to examine the relationship between integrin coding variation and CNS 5-HT function.

The reduced exploratory and social behaviors, and blood hyperserotonemia observed in KI males are all core phenotypes observed in animal models of ASD (Silverman et al., 2010). Integrin αvβ3 interacts functionally and/or physically with multiple proteins associated with ASD, including the plasminogen activator-urokinase receptor (*PLAUR*; Xue et al., 1997; Eagleson et al., 2011), thrombospondin 1 (*THBS1*; Gao et al., 1996; Lu et al., 2014), phosphatase and tensin homolog (*PTEN*; Yoganathan et al., 2000; Frazier et al., 2015), exostosin 1 (*EXT1*; Osterholm et al., 2009; Irie et al., 2012), and SERT (*SLC6A4*; Prasad et al., 2005; Sutcliffe et al., 2005; Carneiro et al., 2008; Veenstra-VanderWeele et al., 2012). Of those functional interaction partners, the behavioral profile of KI mice best recapitulates those observed in multiple models of SERT dysfunction, both genetic and pharmacological (Zhao et al., 2006; Ansorge et al., 2008; Joeyen-Waldorf et al., 2009). The alterations in behaviors in KI mice, including reduced ambulatory activity in the open field, reduced number of

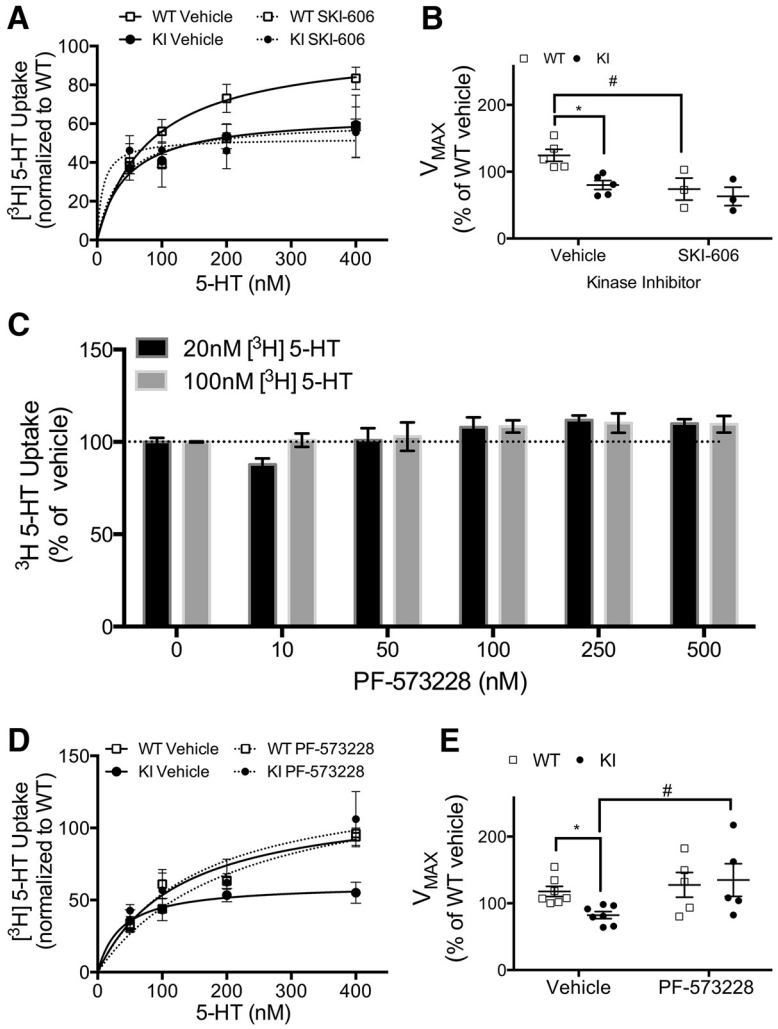

Figure 5. Inhibition of FAK, but not Src, rescues SERT activity in KI mice. Representative kinetic saturation curves of SERT-mediated [^{3}H] 5-HT uptake in WT (□) and KI (■) midbrain synaptoneurosomes treated with vehicle (solid lines) or kinase inhibitors (dashed lines). ***A***, Representative curves for samples treated with vehicle or the Src inhibitor SKI-606 (100 nM). ***B***, Analysis of maximum SERT-mediated 5-HT transport velocity (V_{max}) from kinetic saturation experiments in samples treated with vehicle or SKI-606 (two-way ANOVA SKI-606 effect: $F_{(1,12)} = 7.36$, $p = 0.019$; two-way ANOVA genotype effect: $F_{(1,12)} = 5.53$, $p = 0.036$; Bonferroni-corrected post-test: $WT_{vehicle}$ vs $KI_{vehicle}$, $p = 0.019$; $WT_{vehicle}$ vs WT_{SKI}, $p = 0.026$). Number of animals: WT, $N_{vehicle} = 5$, $N_{SKI} = 3$; KI, $N_{vehicle} = 5$, $N_{SKI} = 3$. ***C***, Concentration-response analyses of the FAK inhibitor PF-573228. SERT-mediated [^{3}H] 5-HT uptake (20 and 100 nM) in WT synaptoneurosomes was measured in the absence or presence of increasing concentrations of PF-573228. Number of animals, 8. ***D***, Representative curves for samples treated with vehicle or the FAK inhibitor PF-573228 (100 nM). ***E***, Analysis of maximum SERT-mediated 5-HT transport velocity (V_{max}) from kinetic saturation experiments in samples treated with vehicle or PF-573228 (100 nM; two-way ANOVA PF-573228 effect: $F_{(1,20)} = 5.05$, $p = 0.036$. Bonferroni-corrected post-test: $KI_{vehicle}$ vs KI_{PF}, $p = 0.029$). Number of animals: WT: $N_{vehicle} = 7$, $N_{PF} = 5$; KI: $N_{vehicle} = 7$, $N_{PF} = 5$. For genotype comparisons: $^*p < 0.05$, and drug comparisons within the same genotype; $\#p < 0.05$.

entries in an open arm of the elevated zero maze, reduced marble burying, and increased immobility time in the tail suspension test, are all observed in models where SERT inactivation is achieved during development but not in adulthood (Zhao et al., 2006; Ansorge et al., 2008; Joeyen-Waldorf et al., 2009). Many of these phenotypes, including alterations in synaptic number and connectivity, likely occur at/during early developmental stages. Identifying the phenotypes caused by alterations in integrin β3 function within 5-HT neurons versus those occurring in other cell types is key to understanding the contribution of this molecule to the etiology of ASD.

Constitutive activation of integrin αvβ3 influences SERT function in the adult animal, effects that can be recapitulated, or reversed, by pharmacologically targeting tyrosine kinases in an *ex vivo* preparation. We observed significant reductions in transport velocity (V_{max}) that did not result from reduced plasma membrane expression, reduced potency, or binding capacity of the transporter. We also found reductions in the number of 5-HT synapses in the midbrain, although no changes in SERT protein levels were observed in tissue or synaptosomes isolated from KI mice when compared with WT preparations, indicating compensatory effects at the neuron level. Together, these data suggest that integrin αvβ3 receptors dynamically regulate SERT uptake activity and point to novel pathways that can be targeted pharmacologically for the amelioration of 5-HT-dependent deficits in adult animals.

Although SERT activity in platelets and the midbrain relies on integrin β3 expression (Carneiro et al., 2008; Mazaloushkas et al., 2015), the effects of signaling downstream of this integrin on SERT function are context dependent. We observed elevated 5-HT levels in the whole blood of KI mice, indicating that the murine Pro32Pro33 integrin β3 subunit variant increases SERT activity in platelets. In midbrain preparations, however, we observed a reduction in SERT uptake activity by the Pro32Pro33 mutation. The magnitude of these changes are also likely different between platelets and brain, as indicated by an ~1.8-fold increase in blood 5-HT/5-HIAA levels compared with an ~1.2-fold increase in the midbrain, although a direct comparison of transport activity was not performed. These differences can be explained by cellular environment, where platelets were studied either in suspension (Carneiro and Blakely, 2006) or after a short-term attachment (Carneiro et al., 2008), whereas here we studied isolated synaptoneurosomes, which maintain stable synaptic and ECM interactions [in addition to expressing different receptors (αIIbβ3 in platelets and αvβ3 in neurons)]. In platelets in suspension, activation of integrin αIIbβ3 via PKC leads to inactivation and internalization of SERT, effects that are mediated by the focal adhesion adaptor protein Hic-5 (Carneiro and Blakely, 2006). On the other hand, activation of platelet integrin αIIbβ3 by fibrinogen binding, or by expression of the human αIIbPro33β3 variant in HEK293 cells (and in platelets) likely enhances transport activity (Carneiro et al., 2008). The immediate canonical signaling pathway activated upon integrin αvβ3 activation is the FAK/Src protein complex (Hynes, 2002). Our previous studies revealed increased Src and decreased FAK phosphorylation in platelets of KI mice, which likely influence SERT activity (Oliver et al., 2014). Other studies have demonstrated that Src-mediated phosphorylation of SERT increases the stability and uptake capacity of the protein (Zarpellon et al., 2008; Annamalai et al., 2012), effects replicated here in WT samples,

but not KI samples. We observed that the inhibition of Src activity only reduces SERT V_{max} in WT synaptoneurosomes, suggesting that Src signaling may be downregulated in KI synapses. On the other hand, our ability to rescue SERT function in KI midbrain synaptoneurosomes by the inhibition of FAK indicates elevated FAK signaling downstream of the Pro32Pro33 mutant, as confirmed by increased pFAK localization in 5-HT synapses. Our data therefore suggest that the Src–FAK pathway is uncoupled by constitutive activation of integrin β3, and thus each kinase may be influencing SERT independently. The context-dependent nature of SERT regulation is underscored by the loss of colocalization of SERT with focal adhesion proteins in KI synapses. This indicates that the association of SERT with integrin signaling complexes is not necessary for the regulation of the transporter by constitutive signaling downstream of the "primed" Pro32Pro33 mutant.

In conclusion, our results (1) provide evidence of functional regulation of the 5-HT system by the Leu33Pro coding variant of integrin β3 and (2) identify signaling mechanisms by which this interaction exerts its effects. While we achieved pharmacological rescue of SERT activity *ex vivo*, pharmacological rescue of the behavioral phenotypes will go a long way toward clarifying the molecular underpinnings of the emotional, social, and repetitive behaviors affected by this mutation. Our studies support the contention that the integrin αvβ3 receptor may represent a central member of presynaptic and postsynaptic protein networks that influence the risk for neuropsychiatric conditions.

References

Allen JR, Ross ST, Davidson MW (2014) Structured illumination microscopy for superresolution. Chemphyschem 15:566–576. CrossRef Medline

Annamalai B, Mannangatti P, Arapulisamy O, Shippenberg TS, Jayanthi LD, Ramamoorthy S (2012) Tyrosine phosphorylation of the human serotonin transporter: a role in the transporter stability and function. Mol Pharmacol 81:73–85. CrossRef Medline

Ansorge MS, Morelli E, Gingrich JA (2008) Inhibition of serotonin but not norepinephrine transport during development produces delayed, persistent perturbations of emotional behaviors in mice. J Neurosci 28:199–207. CrossRef Medline

Arias-Vásquez A, Altink ME, Rommelse NN, Slaats-Willemse DI, Buschgens CJ, Fliers EA, Faraone SV, Sergeant JA, Oosterlaan J, Franke B, Buitelaar JK (2011) CDH13 is associated with working memory performance in attention deficit/hyperactivity disorder. Genes Brain Behav 10:844–851. CrossRef Medline

Banerjee E, Nandagopal K (2015) Does serotonin deficit mediate susceptibility to ADHD? Neurochem Int 82:52–68. CrossRef Medline

Blaess S, Graus-Porta D, Belvindrah R, Radakovits R, Pons S, Littlewood-Evans A, Senften M, Guo H, Li Y, Miner JH, Reichardt LF, Müller U (2004) β1-integrins are critical for cerebellar granule cell precursor proliferation. J Neurosci 24:3402–3412. CrossRef Medline

Blakely RD, Ramamoorthy S, Schroeter S, Qian Y, Apparsundaram S, Galli A, DeFelice LJ (1998) Regulated phosphorylation and trafficking of antidepressant-sensitive serotonin transporter proteins. Biol Psychiatry 44:169–178. CrossRef Medline

Brocco M, Dekeyne A, Veiga S, Girardon S, Millan MJ (2002) Induction of hyperlocomotion in mice exposed to a novel environment by inhibition of serotonin reuptake. A pharmacological characterization of diverse classes of antidepressant agents. Pharmacol Biochem Behav 71:667–680. CrossRef Medline

Cabodi S, Di Stefano P, Leal Mdel P, Tinnirello A, Bisaro B, Morello V, Damiano L, Aramu S, Repetto D, Tornillo G, Defilippi P (2010) Integrins and signal transduction. Adv Exp Med Biol 674:43–54. CrossRef Medline

Carneiro AM, Blakely RD (2006) Serotonin-, protein kinase C-, and Hic-5-associated redistribution of the platelet serotonin transporter. J Biol Chem 281:24769–24780. CrossRef Medline

Carneiro AM, Cook EH, Murphy DL, Blakely RD (2008) Interactions between integrin alphaIIbbeta3 and the serotonin transporter regulate serotonin transport and platelet aggregation in mice and humans. J Clin Invest 118:1544–1552. CrossRef Medline

Carter MD, Shah CR, Muller CL, Crawley JN, Carneiro AM, Veenstra-VanderWeele J (2011) Absence of preference for social novelty and increased grooming in integrin beta3 knockout mice: initial studies and future directions. Autism Res 4:57–67. CrossRef Medline

Ciccone MA, Timmons M, Phillips A, Quick MW (2008) Calcium/calmodulin-dependent kinase II regulates the interaction between the serotonin transporter and syntaxin 1A. Neuropharmacology 55:763–770. CrossRef Medline

Clegg DO, Wingerd KL, Hikita ST, Tolhurst EC (2003) Integrins in the development, function and dysfunction of the nervous system. Front Biosci 8:d723–d750. CrossRef Medline

Cook EH, Leventhal BL (1996) The serotonin system in autism. Curr Opin Pediatr 8:348–354. CrossRef Medline

Coutinho AM, Sousa I, Martins M, Correia C, Morgadinho T, Bento C, Marques C, Ataíde A, Miguel TS, Moore JH, Oliveira G, Vicente AM (2007) Evidence for epistasis between SLC6A4 and ITGB3 in autism etiology and in the determination of platelet serotonin levels. Hum Genet 121:243–256. CrossRef Medline

Cryan JF, Holmes A (2005) The ascent of mouse: advances in modelling human depression and anxiety. Nat Rev Drug Discov 4:775–790. CrossRef Medline

Cryan JF, Mombereau C, Vassout A (2005a) The tail suspension test as a model for assessing antidepressant activity: review of pharmacological and genetic studies in mice. Neurosci Biobehav Rev 29:571–625. CrossRef Medline

Cryan JF, Valentino RJ, Lucki I (2005b) Assessing substrates underlying the behavioral effects of antidepressants using the modified rat forced swimming test. Neurosci Biobehav Rev 29:547–569. CrossRef Medline

Denny JC, Ritchie MD, Basford MA, Pulley JM, Bastarache L, Brown-Gentry K, Wang D, Masys DR, Roden DM, Crawford DC (2010) PheWAS: demonstrating the feasibility of a phenome-wide scan to discover gene-disease associations. Bioinformatics 26:1205–1210. CrossRef Medline

Denny JC, Crawford DC, Ritchie MD, Bielinski SJ, Basford MA, Bradford Y, Chai HS, Bastarache L, Zuvich R, Peissig P, Carrell D, Ramirez AH, Pathak J, Wilke RA, Rasmussen L, Wang X, Pacheco JA, Kho AN, Hayes MG, Weston N, Matsumoto M, Kopp PA, Newton KM, Jarvik GP, Li R, Manolio TA, Kullo IJ, Chute CG, Chisholm RL, Larson EB, McCarty CA, Masys DR, Roden DM, de Andrade M (2011) Variants near FOXE1 are associated with hypothyroidism and other thyroid conditions: using electronic medical records for genome- and phenome-wide studies. Am J Hum Genet 89:529–542. CrossRef Medline

Denny JC, Bastarache L, Ritchie MD, Carroll RJ, Zink R, Mosley JD, Field JR, Pulley JM, Ramirez AH, Bowton E, Basford MA, Carrell DS, Peissig PL, Kho AN, Pacheco JA, Rasmussen LV, Crosslin DR, Crane PK, Pathak J, Bielinski SJ, Pendergrass SA, Xu H, Hindorff LA, Li R, Manolio TA, Chute CG, Chisholm RL, Larson EB, Jarvik GP, Brilliant MH, McCarty CA, Kullo IJ, Haines JL, Crawford DC, Masys DR, Roden DM (2013) Systematic comparison of phenome-wide association study of electronic medical record data and genome-wide association study data. Nat Biotechnol 31:1102–1110. CrossRef Medline

Eagleson KL, Campbell DB, Thompson BL, Bergman MY, Levitt P (2011) The autism risk genes MET and PLAUR differentially impact cortical development. Autism Res 4:68–83. CrossRef Medline

Frazier TW, Embacher R, Tilot AK, Koenig K, Mester J, Eng C (2015) Molecular and phenotypic abnormalities in individuals with germline heterozygous PTEN mutations and autism. Mol Psychiatry 20:1132–1138. CrossRef Medline

Gao AG, Lindberg FP, Dimitry JM, Brown EJ, Frazier WA (1996) Thrombospondin modulates alpha v beta 3 function through integrin-associated protein. J Cell Biol 135:533–544. CrossRef Medline

Gu WL, Fu SL, Wang YX, Li Y, Lü HZ, Xu XM, Lu PH (2009) Chondroitin sulfate proteoglycans regulate the growth, differentiation and migration of multipotent neural precursor cells through the integrin signaling pathway. BMC Neurosci 10:128. CrossRef Medline

Health Care Financing Administration (1990) ICD-9-CM: international classification of diseases, 9th revision, clinical modification, third edition, volumes 1 and 2: official authorized addendum, effective October 1, 1990. Washington, DC: US Government Printing Office.

Hynes RO (2002) Integrins: bidirectional, allosteric signaling machines. Cell 110:673–687. CrossRef Medline

Irie F, Badie-Mahdavi H, Yamaguchi Y (2012) Autism-like socio-communi-

cative deficits and stereotypies in mice lacking heparan sulfate. Proc Natl Acad Sci U S A 109:5052–5056. CrossRef Medline

Jaiswal P, Guhathakurta S, Singh AS, Verma D, Pandey M, Varghese M, Sinha S, Ghosh S, Mohanakumar KP, Rajamma U (2015) SLC6A4 markers modulate platelet 5-HT level and specific behaviors of autism: a study from an Indian population. Prog Neuropsychopharmacol Biol Psychiatry 56:196–206. CrossRef Medline

Jallu V, Poulain P, Fuchs PF, Kaplan C, de Brevern AG (2012) Modeling and molecular dynamics of HPA-1a and -1b polymorphisms: effects on the structure of the beta3 subunit of the alphaIIbbeta3 integrin. PLoS One 7:e47304. CrossRef Medline

Joel D, Weiner I (2000) The connections of the dopaminergic system with the striatum in rats and primates: an analysis with respect to the functional and compartmental organization of the striatum. Neuroscience 96:451–474. CrossRef Medline

Joeyen-Waldorf J, Edgar N, Sibille E (2009) The roles of sex and serotonin transporter levels in age- and stress-related emotionality in mice. Brain Res 1286:84–93. CrossRef Medline

Kent L, Emerton J, Bhadravathi V, Weisblatt E, Pasco G, Willatt LR, McMahon R, Yates JR (2008) X-linked ichthyosis (steroid sulfatase deficiency) is associated with increased risk of attention deficit hyperactivity disorder, autism and social communication deficits. J Med Genet 45:519–524. CrossRef Medline

Lasky-Su J, Neale BM, Franke B, Anney RJ, Zhou K, Maller JB, Vasquez AA, Chen W, Asherson P, Buitelaar J, Banaschewski T, Ebstein R, Gill M, Miranda A, Mulas F, Oades RD, Roeyers H, Rothenberger A, Sergeant J, Sonuga-Barke E, Steinhausen HC, Taylor E, Daly M, Laird N, Lange C, Faraone SV (2008) Genome-wide association scan of quantitative traits for attention deficit hyperactivity disorder identifies novel associations and confirms candidate gene associations. Am J Med Genet B Neuropsychiatr Genet 147B:1345–1354. CrossRef Medline

Lu L, Guo H, Peng Y, Xun G, Liu Y, Xiong Z, Tian D, Liu Y, Li W, Xu X, Zhao J, Hu Z, Xia K (2014) Common and rare variants of the THBS1 gene associated with the risk for autism. Psychiatr Genet 24:235–240. CrossRef Medline

Ma DQ, Rabionet R, Konidari I, Jaworski J, Cukier HN, Wright HH, Abramson RK, Gilbert JR, Cuccaro ML, Pericak-Vance MA, Martin ER (2010) Association and gene-gene interaction of SLC6A4 and ITGB3 in autism. Am J Med Genet B Neuropsychiatr Genet 153B:477–483. CrossRef Medline

Mazalouskas M, Jessen T, Varney S, Sutcliffe JS, Veenstra-VanderWeele J, Cook EH Jr, Carneiro AM (2015) Integrin beta3 haploinsufficiency modulates serotonin transport and antidepressant-sensitive behavior in mice. Neuropsychopharmacology 40:2015–2024. CrossRef Medline

McGeachie AB, Cingolani LA, Goda Y (2011) Stabilising influence: integrins in regulation of synaptic plasticity. Neurosci Res 70:24–29. CrossRef Medline

Muller CL, Anacker AMJ, Veenstra-VanderWeele J (2016) The serotonin system in autism spectrum disorder: from biomarker to animal models. Neuroscience 321:24–41. CrossRef Medline

Murase S, Owens DF, McKay RD (2011) In the newborn hippocampus, neurotrophin-dependent survival requires spontaneous activity and integrin signaling. J Neurosci 31:7791–7800. CrossRef Medline

Napolioni V, Lombardi F, Sacco R, Curatolo P, Manzi B, Alessandrelli R, Militerni R, Bravaccio C, Lenti C, Saccani M, Schneider C, Melmed R, Pascucci T, Puglisi-Allegra S, Reichelt KL, Rousseau F, Lewin P, Persico AM (2011) Family-based association study of ITGB3 in autism spectrum disorder and its endophenotypes. Eur J Hum Genet 19:353–359. CrossRef Medline

Oliver KH, Jessen T, Crawford EL, Chung CY, Sutcliffe JS, Carneiro AM (2014) Pro32Pro33 mutations in the integrin beta3 PSI domain result in alphaIIbbeta3 priming and enhanced adhesion: reversal of the hypercoagulability phenotype by the Src inhibitor SKI-606. Mol Pharmacol 85:921–931. CrossRef Medline

Osterholm C, Barczyk MM, Busse M, Grønning M, Reed RK, Kusche-Gullberg M (2009) Mutation in the heparan sulfate biosynthesis enzyme EXT1 influences growth factor signaling and fibroblast interactions with the extracellular matrix. J Biol Chem 284:34935–34943. CrossRef Medline

Oved K, Morag A, Pasmanik-Chor M, Rehavi M, Shomron N, Gurwitz D (2013) Genome-wide expression profiling of human lymphoblastoid cell lines implicates integrin beta-3 in the mode of action of antidepressants. Transl Psychiatry 3:e313. CrossRef Medline

Phillips GR, Huang JK, Wang Y, Tanaka H, Shapiro L, Zhang W, Shan WS, Arndt K, Frank M, Gordon RE, Gawinowicz MA, Zhao Y, Colman DR (2001) The presynaptic particle web: ultrastructure, composition, dissolution, and reconstitution. Neuron 32:63–77. CrossRef Medline

Prasad HC, Zhu CB, McCauley JL, Samuvel DJ, Ramamoorthy S, Shelton RC, Hewlett WA, Sutcliffe JS, Blakely RD (2005) Human serotonin transporter variants display altered sensitivity to protein kinase G and p38 mitogen-activated protein kinase. Proc Natl Acad Sci U S A 102:11545–11550. CrossRef Medline

Quick MW (2002) Role of syntaxin 1A on serotonin transporter expression in developing thalamocortical neurons. Int J Dev Neurosci 20:219–224. CrossRef Medline

Rivero O, Selten MM, Sich S, Popp S, Bacmeister L, Amendola E, Negwer M, Schubert D, Proft F, Kiser D, Schmitt AG, Gross C, Kolk SM, Strekalova T, van den Hove D, Resink TJ, Nadif Kasri N, Lesch KP (2015) Cadherin-13, a risk gene for ADHD and comorbid disorders, impacts GABAergic function in hippocampus and cognition. Transl Psychiatry 5:e655. CrossRef Medline

Roden DM, Pulley JM, Basford MA, Bernard GR, Clayton EW, Balser JR, Masys DR (2008) Development of a large-scale de-identified DNA biobank to enable personalized medicine. Clin Pharmacol Ther 84:362–369. CrossRef Medline

Ruhé HG, Mason NS, Schene AH (2007) Mood is indirectly related to serotonin, norepinephrine and dopamine levels in humans: a meta-analysis of monoamine depletion studies. Mol Psychiatry 12:331–359. CrossRef Medline

Salatino-Oliveira A, Genro JP, Polanczyk G, Zeni C, Schmitz M, Kieling C, Anselmi L, Menezes AM, Barros FC, Polina ER, Mota NR, Grevet EH, Bau CH, Rohde LA, Hutz MH (2015) Cadherin-13 gene is associated with hyperactive/impulsive symptoms in attention/deficit hyperactivity disorder. Am J Med Genet B Neuropsychiatr Genet 168B:162–169. CrossRef Medline

Sathyanesan A, Ogura T, Lin W (2012) Automated measurement of nerve fiber density using line intensity scan analysis. J Neurosci Methods 206:165–175. CrossRef Medline

Schatzberg AF (2000) Clinical efficacy of reboxetine in major depression. J Clin Psychiatry 61 [Suppl 10]:31–38.

Silverman JL, Yang M, Lord C, Crawley JN (2010) Behavioural phenotyping assays for mouse models of autism. Nat Rev Neurosci 11:490–502. CrossRef Medline

Singh AS, Chandra R, Guhathakurta S, Sinha S, Chatterjee A, Ahmed S, Ghosh S, Rajamma U (2013) Genetic association and gene-gene interaction analyses suggest likely involvement of ITGB3 and TPH2 with autism spectrum disorder (ASD) in the Indian population. Prog Neuropsychopharmacol Biol Psychiatry 45:131–143. CrossRef Medline

Sutcliffe JS, Delahanty RJ, Prasad HC, McCauley JL, Han Q, Jiang L, Li C, Folstein SE, Blakely RD (2005) Allelic heterogeneity at the serotonin transporter locus (SLC6A4) confers susceptibility to autism and rigid-compulsive behaviors. Am J Hum Genet 77:265–279. CrossRef Medline

Thakker DR, Natt F, Hüsken D, van der Putten H, Maier R, Hoyer D, Cryan JF (2005) siRNA-mediated knockdown of the serotonin transporter in the adult mouse brain. Mol Psychiatry 10:782–789, 714. CrossRef Medline

Tzanoulinou S, García-Mompó C, Riccio O, Grosse J, Zanoletti O, Dedousis P, Nacher J, Sandi C (2016) Neuroligin-2 expression in the prefrontal cortex is involved in attention deficits induced by peripubertal stress. Neuropsychopharmacology 41:751–761. CrossRef Medline

Veenstra-VanderWeele J, Muller CL, Iwamoto H, Sauer JE, Owens WA, Shah CR, Cohen J, Mannangatti P, Jessen T, Thompson BJ, Ye R, Kerr TM, Carneiro AM, Crawley JN, Sanders-Bush E, McMahon DG, Ramamoorthy S, Daws LC, Sutcliffe JS, Blakely RD (2012) Autism gene variant causes hyperserotonemia, serotonin receptor hypersensitivity, social impairment and repetitive behavior. Proc Natl Acad Sci U S A 109:5469–5474. CrossRef Medline

Vijayan KV, Huang TC, Liu Y, Bernardo A, Dong JF, Goldschmidt-Clermont PJ, Alevriadou BR, Bray PF (2003a) Shear stress augments the enhanced adhesive phenotype of cells expressing the Pro33 isoform of integrin beta3. FEBS Lett 540:41–46. CrossRef Medline

Vijayan KV, Liu Y, Dong JF, Bray PF (2003b) Enhanced activation of mitogen-activated protein kinase and myosin light chain kinase by the Pro33 polymorphism of integrin beta 3. J Biol Chem 278:3860–3867. CrossRef Medline

Weiss LA, Veenstra-Vanderweele J, Newman DL, Kim SJ, Dytch H, McPeek MS, Cheng S, Ober C, Cook EH Jr, Abney M (2004) Genome-wide as-

sociation study identifies ITGB3 as a QTL for whole blood serotonin. Eur J Hum Genet 12:949–954. CrossRef Medline

Weiss LA, Kosova G, Delahanty RJ, Jiang L, Cook EH, Ober C, Sutcliffe JS (2006a) Variation in ITGB3 is associated with whole-blood serotonin level and autism susceptibility. Eur J Hum Genet 14:923–931. CrossRef Medline

Weiss LA, Ober C, Cook EH Jr (2006b) ITGB3 shows genetic and expression interaction with SLC6A4. Hum Genet 120:93–100. CrossRef Medline

Wersinger C, Rusnak M, Sidhu A (2006) Modulation of the trafficking of the human serotonin transporter by human alpha-synuclein. Eur J Neurosci 24:55–64. CrossRef Medline

Whitney MS, Shemery AM, Yaw AM, Donovan LJ, Glass JD, Deneris ES (2016) Adult brain serotonin deficiency causes hyperactivity, circadian disruption, and elimination of siestas. J Neurosci 36:9828–9842. CrossRef Medline

Whyte A, Jessen T, Varney S, Carneiro AM (2014) Serotonin transporter and integrin beta 3 genes interact to modulate serotonin uptake in mouse brain. Neurochem Int 73:122–126. CrossRef Medline

Xue W, Mizukami I, Todd RF 3rd, Petty HR (1997) Urokinase-type plasminogen activator receptors associate with beta1 and beta3 integrins of fibrosarcoma cells: dependence on extracellular matrix components. Cancer Res 57:1682–1689. Medline

Yoganathan TN, Costello P, Chen X, Jabali M, Yan J, Leung D, Zhang Z, Yee A, Dedhar S, Sanghera J (2000) Integrin-linked kinase (ILK): a "hot" therapeutic target. Biochem Pharmacol 60:1115–1119. CrossRef Medline

Zarpellon A, Donella-Deana A, Folda A, Turetta L, Pavanetto M, Deana R (2008) Serotonin (5-HT) transport in human platelets is modulated by Src-catalysed Tyr-phosphorylation of the plasma membrane transporter SERT. Cell Physiol Biochem 21:87–94. CrossRef Medline

Zhao S, Edwards J, Carroll J, Wiedholz L, Millstein RA, Jaing C, Murphy DL, Lanthorn TH, Holmes A (2006) Insertion mutation at the C-terminus of the serotonin transporter disrupts brain serotonin function and emotion-related behaviors in mice. Neuroscience 140:321–334. CrossRef Medline

Zhu CB, Lindler KM, Campbell NG, Sutcliffe JS, Hewlett WA, Blakely RD (2011) Colocalization and regulated physical association of presynaptic serotonin transporters with A(3) adenosine receptors. Mol Pharmacol 80:458–465. CrossRef Medline

Zohar J, Westenberg HG (2000) Anxiety disorders: a review of tricyclic antidepressants and selective serotonin reuptake inhibitors. Acta Psychiatr Scand Suppl 403:39–49. Medline

Zohar J, Amital D, Cropp HD, Cohen-Rappaport G, Zinger Y, Sasson Y (2000a) Update on the epidemiology, diagnosis, and treatment of post-traumatic stress disorder. Dialogues Clin Neurosci 2:37–43. Medline

Zohar J, Chopra M, Sasson Y, Amiaz R, Amital D (2000b) Obsessive compulsive disorder: serotonin and beyond. World J Biol Psychiatry 1:92–100. CrossRef Medline